MAREES TERRESTRES

BULLETIN D'INFORMATIONS

INTERNATIONAL CENTER FOR EARTH TIDES
CENTRE INTERNATIONAL DES MAREES TERRESTRES

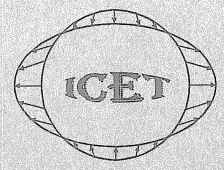

Federation of Astronomical and Geophysical Data Analysis Services
(FAGS)

International Association of Geodesy - International Gravity Field Service
(IAG – IGFS)

Publié avec le soutien de l'Observatoire Royal de Belgique

BIM
1 3 8

15 DECEMBRE 2003

Editeur: Dr. Bernard DUCARME
Observatoire Royal de Belgique
Avenue Circulaire 3
B-1180 Bruxelles

International Association of Geodesy

15th International Symposium on Earth Tides
2-6 August 2004
Ottawa, Canada

Conveners
International Association of Geodesy & IAG Earth Tides Subcommission

The 15th international Symposium on Earth Tides will be held in Ottawa, Canada's Capital, from 2-6 August 2004. Ottawa is the heart of Canada, and much more than just a beautiful and spectacular city. With its neo-Gothic style and spirit, Ottawa straddles the border of the provinces of Ontario and Quebec exactly where Ottawa, Gatineau and Rideau rivers converge. Ottawa is the cultural and festival city with the highest concentration of museums in Canada. Parklands, gardens, trails, recreational pathways, historic monuments and grounds, and the Rideau Canal offer visitors an unsurpassed blend of national pride and French and English culture.

The National Arts Centre (NAC) will be the venue of the conference. It is among the largest performing arts complexes in Canada and is situated in the heart of the nation's capital across from Confederation Square and Parliament Hill, right next to Rideau Canal. NAC is unique, for it is the only multidisciplinary and bilingual performing arts centre in North America and features one of the largest stages on the continent.

In order to help us plan and organise the conference and keep you informed, we kindly ask you to fill out and submit the on-line form on the website http://www.yorku.ca/ets. Information on travel, accommodation, registration and call for papers will be posted there. If you require assistance please e-mail us. We'll be glad to help!

Local Organizing Committee

Dr. Spiros Pagiatakis (Chair, York University, spiros@yorku.ca)
Dr. Joseph Henton (Geodetic Survey Division, NRCan, jhenton@nrcan.gc.ca)
Dr. Anthony Lambert (Geological Survey of Canada, NRCan, tlambert@nrcan.gc.ca)
Mr. Jacques Liard (Geodetic Survey Division, NRCan, jliard@nrcan.gc.ca)
Dr. Lalu Mansinha (University of Western Ontario, lalu@uwo.ca)
Dr. James Merriam (University of Saskatchewan, merriam@duke.usask.ca)
Dr. Douglas Smylie (York University, doug@core.yorku.ca)
Ms. Margaret-Anne Stroh (Conference Concepts, mastroh@telus.net)

BIM 138

15 décembre 2003

IN MEMORIAM

Professor Tadeusz Chojnicki, (1932 – 2003).

On 7 September 2003 our colleague and friend Professor Tadeusz Chojnicki, the member of the Department of the Planetary Geodesy of the Space Research Centre of the Polish Academy of Sciences, passed away after the long and grave disease.

He started his scientific career in the Institute of Geodesy and Cartography, the Gravimetric Laboratory where he participated in establishing of the gravity network of Poland and the preparation of the map of gravity anomalies. There, he encountered first time the problem of the Earth's tides that became the topic of his research until the end of his days.

In 1966 he moved to the Polish Academy of Sciences, where he was invited to organize the research group on Earth's tides. The late Director of the Planetary Geodesy Laboratory, Professor Ludosław Cichowicz, requested him to create the modern tidal service in Poland and to establish the international cooperation with the world laboratories leading in this domain. He started with the organization of the measurement station of tides in the basement of the Palace of Science and Culture, the tallest building in Warsaw. The station was equipped with the Ascania gravimeter adapted to the permanent service in stable conditions. The station started its operation in 1968. However, the really great achievement of Chojnicki in the field of tides was the elaboration of the method of analysis of the tidal data based on the Gauss least squares rule. In 1977 he published his work "Sur l'analyse des observations de marees terrestres" where the method is described. Very soon, it was accepted by Professor Paul Melchior, the Director of the International Earth Tides Service, as the standard method for the tidal data analysis.

In 1970 Tadeusz Chojnicki started with the organization of the tidal observatory in the caves of the Ksiaz Castle, in Silesia, South West of Poland. This unique place offered some particular advantages for the investigation of the Earth crust. In cooperation with French and German experts the modern instruments were installed, including horizontal pendulum tiltmeters and gravimeters. Today, this Observatory belongs to the first rank of the world tidal stations.

Chojnicki combined his skill of instrumental inventiveness with the ingenuity in theory and methodology in a very creative way. It helped him to discover some new effects in Earth tides: the resonance of tidal waves of plumb line variations with the earth core as well as seasonal and non-seasonal modulation of tidal waves. These phenomena have been detected on the base of many years long series of plumb line variations from Ksiaz Observatory. In 1984 Chojnicki created the new tidal station equipped with the LaCoste&Romberg gravimeter in the building of the Space Research Centre in Warsaw in the building of the Space Research Centre in Warsaw. Data from both stations were constantly provided to the International Centre for Earth Tides. Prof. Chojnicki helped to develop the research of the Earth tides in other institutes in Poland and abroad, too.

Professor Tadeusz Chojnicki was an author of above hundred of scientific publications. During his life he was a member of numerous scientific commissions and committees, national and international. In last years he was active in the Scientific Council of the Space Research Centre and the Institute of Geophysics of the Polish Academy of Sciences. He was awarded with the Knight Cross of the Polonia Restituta Order, the Golden Cross of Merit and the Medal of Merits for Geodesy and Cartography.

Not only he was the prominent scientist but also the exceptional personality. His liking for music, poetry and arts made him the desired participant of any meeting, scientific or social. His sense of humor was helpful in the hard reality of the everyday life.

We, his colleagues from the Space Research Centre of the Polish Academy of Sciences, will remember his invaluable contribution to our joint work and to the geodesy in Poland and in the world.

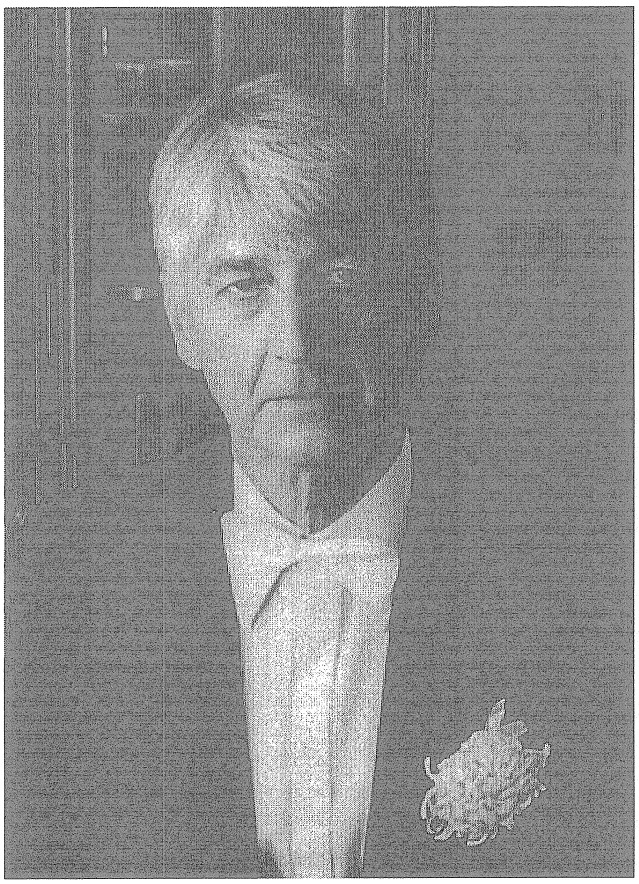

An Introduction to the use of HICUM for Signal Analysis

M. van Ruymbeke (1), R. Howard(1), E. Pütz(1), Fr. Beauducel (2)*
A. Somerhausen (1) and J- P. Barriot (3)
1 Royal Observatory of Belgium, Avenue Circulaire,3 B-1180 Bruxelles, Belgium
2 Institute de Physique du Globe, Place Jussieu, F-75252.Paris Cedex 05 France
3 Bureau Gravimétrique International, Observatoire Midi Pyrénées
14, Av Edouard Belin, 31400 Toulouse Tel 33(0)561332894
**LABVRUY@OMA.BE*

Abstract

This paper introduces a novel method for signal analysis whereby a weak signal can be detected in a noisy environment, providing the time period is known. The time period for each earth tide signal is found using the Doodson argument. Each cycle is then divided into sectors and a histogram of the data is plotted. The histograms for all the cycles are then stacked to produce the cumulative effect, hence the name for the method is HiCum . The paper uses synthetic data to demonstrate the ability of the technique to detect a signal in a noisy environment. Some of the additional benefits of the method over spectrum analysis are shown using field data from EDAS. There is also a section which gives some practical guidance on how to use HiCum with μDAS Grapher.

Keywords: Earth Tides, EDAS, Signal Analysis, Stacking.

1 Introduction

The following is a description of HiCum (Histograms Cumulation), an alternative method of signal analysis, which has been developed to work with the EDAS system by van Ruymbeke et al. (2001). HiCum, like Spectrum Analysis, analyses signal signatures based on Fourier Analysis. Whereas Spectrum Analysis is necessary when the frequency of the signal is not known, in situations where the time period is clearly defined, such as diurnal fluctuations, then the HiCum method is more accurate and is capable of extracting information that would be lost during Spectrum Analysis. It is therefore a powerful tool in monitoring the complex interactions induced by tectonic activities. Here computer generated data is used to test the accuracy of the method and to demonstrate its usefulness. Also included in the text is some practical guidance on the use of the software program, μDAS Grapher, in which HiCum has been embedded.

2 Background Theory

Fourier's Theorem states that any periodic function can be expressed as a sum of sine waves.

$$f(x)= \Sigma (a \cos rx + b \sin rx) + \tfrac{1}{2}c \qquad (1)$$

where r takes integral values and a, b, c are constants.

It can be used as a method of determining the harmonic components of a complex periodic function. Since equation (1) is unchanged by replacing x by $x + 2k\pi$, where k is an integer, it necessarily represents a periodic function in x of period 2π. Consequently in discussing series of this type it is sufficient to consider any interval of width 2π or 360°.

Thus if we have a signal that varies over a period of time, and we can clearly define the frequency, $\omega/2\pi$, then we can equate that to the interval 2π (or 360°) and equation (1) becomes:

$$f(x)= \Sigma (a \cos\omega t + b \sin\omega t) + \tfrac{1}{2}c \qquad (2)$$

Where t is the instantaneous time.
With ω clearly defined, the various harmonics of the system can be found.

HiCum has been developed to analyse data linked with tidal phenomenon (e.g. M2) where the time period can be accurately defined and is stable. HiCum has several advantages over Spectrum Analysis in extracting information where there are complex interactions in a multi parameter environment. Using HiCum the parameters of the fundamental sine wave, the harmonics and any non linearity in the signal can be detected on weak signals with high noise levels.

3 EDAS

Using EDAS, numerous readings from several diverse sensors can be taken at frequent intervals (e.g. every minute) over long periods of time (months) and stored in ASCII files. These files can be analysed at leisure using the software package μDAS Grapher, which has been specifically created for the EDAS files. To further simplify the analysis of the data the Histograms Cumulation (HiCum) method has been incorporated in the μDAS Grapher software package. Its objective is to put forward a graphical display of the behaviour of the non-linearities recorded by the sensors.

4 HiCum

The inspiration for HiCum came from the field of meteorology where stacking data has been used for many decades e.g. Emter et al (1985), following Bartel's work in 1938. A summary of work on a complementary method is given by Zürn and Rydelek This stacking method is the foundation of the HiCum method. A signal, which at first sight appears to be a white noise signal has its time base divided into a series of constant length time periods. The selected time period will be that which is suspected to have an influence on the parameters in question e.g. the M2-wave for gravimetric data. This time period is, by definition, equivalent to an interval of width 2π or 360°. For each period 360 sectors of 1° histogram are created and then the results from each time period are synchronised, normalised by the number of events in each sector and the results from the same time period each day are added, stacked, resulting in an averaging effect producing a picture of the variations, in relation to the wave selected (M2). Once the shape of the histogram for that time period is established the parameters (i.e. Phase and Amplitude) can be computed. Figure 1 is the schematic of the method.

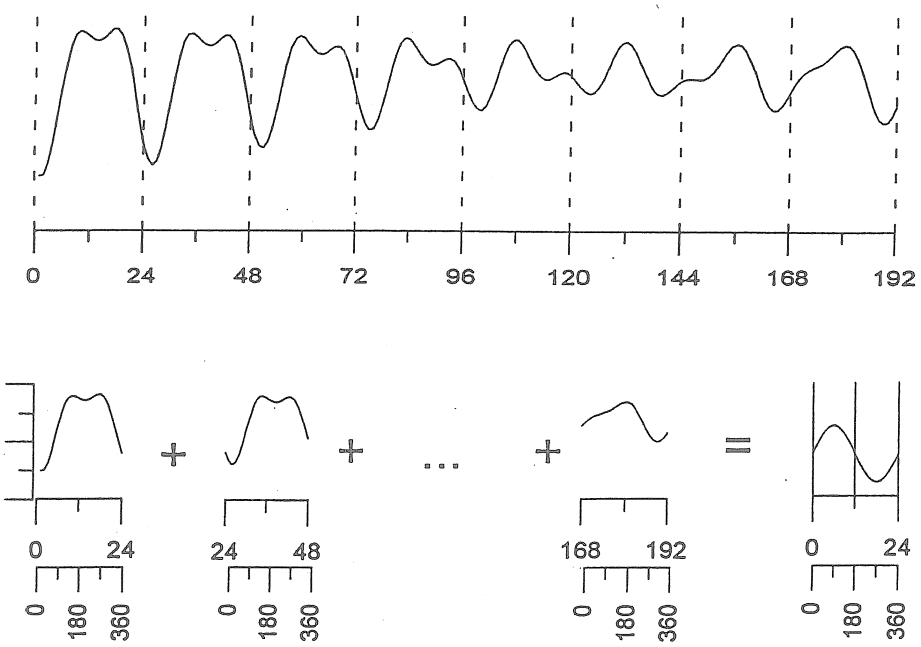

Fig. 1. Principle of HiCum Stacking applied to an eight day gravimeter signal (hourly scale). The series is cut in constant length time intervals corresponding to the period selected by a Doodson argument (i.e. 360° for 24 hours S1 period). The obtained histograms are simply added to obtain an average signal of the concerned component.

Once the fundamental sine wave has been detected it can then removed and the residual data checked for any non-linearity or harmonics. The program gives the option of removing up to four harmonics from the main signal, leaving only the non-linear residuals.

5 Use of Computer Generated Data to Check Accuracy of Method

In order to prove the accuracy of the method a series of known cosine waves and noise signals were computer generated, mixed and transferred to μDAS Grapher. The signals were then analysed using HiCum to see if the individual original waveforms could be detected.

5.1 The first scenario was a mixture of two cosine waves,

$$\cos\omega t + \cos\acute{\omega} t \qquad \text{where } \frac{d\,\omega}{\omega} = 0.035$$

On entering the period for the first wave, cosωt, HiCum should be able to detect that wave and pick up little of the second wave and conversely when the period for cosώt is analysed cosώt should be detected and little from the first wave.

Waves of time period S2 and M2 were used. They were constructed from 40320 data points, which is equivalent to a reading every minute for a lunar month. HiCum was then applied using first the time period for the S2 wave.

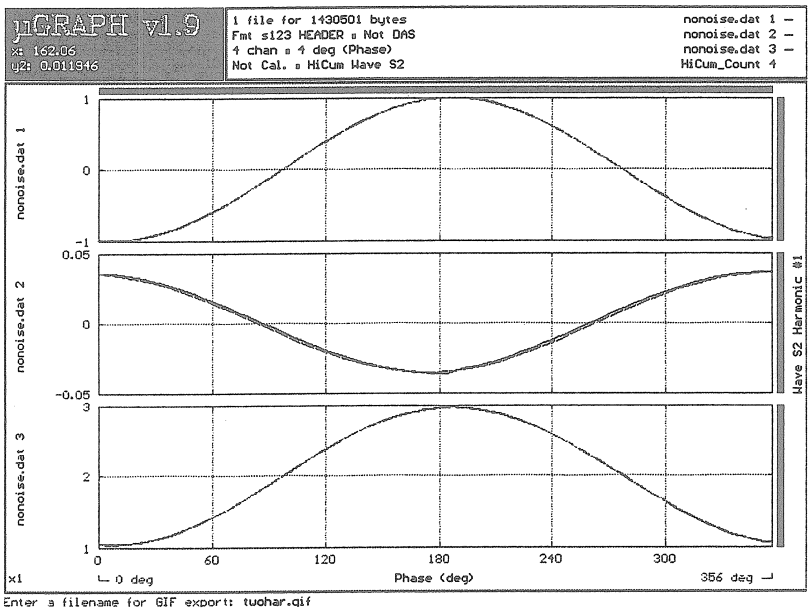

Figure 2 The top graph shows the signal detected from the pure S2 wave, the middle graph shows the signal detected from the M2 wave on the S2time period and the bottom shows the signal detected from a mixture of the S2 and M2 wave, all using a time period of S2.

Figure 2 clearly shows that the first wave, which has phase angle of -173° and an amplitude of 0.965431, is detected from a mixture of the two signals with a phase angle of -173° and an amplitude of 0.965431, the second wave (M2) is detected with a phase angle of -006° and an amplitude of 0.0354039.

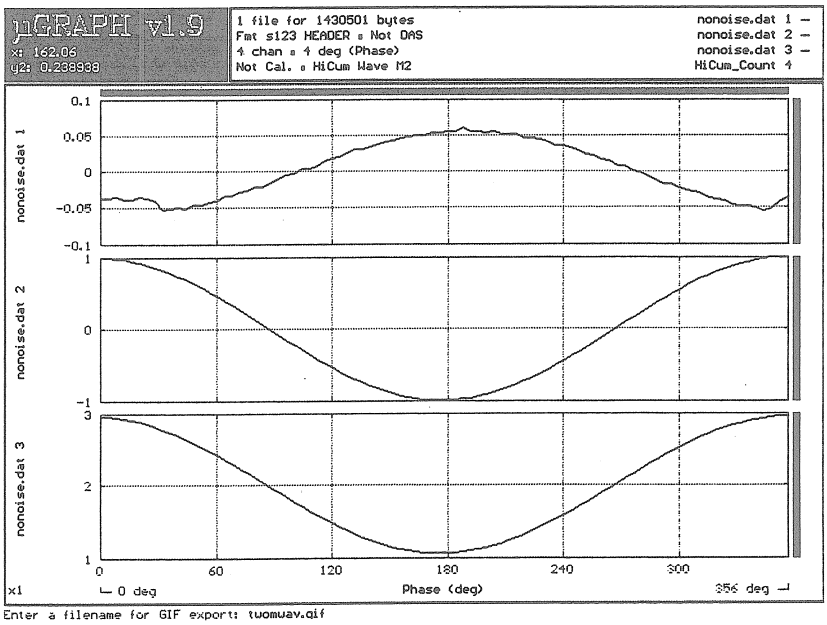

Figure 3 The top graph shows the signal detected from the S2 wave on the M2 period, the middle graph shows the signal from the M2 wave and the bottom shows the signal detected from a mixture of the S2 and M2 wave using a time period of M2.

Figure 3 shows that with M2 time period applied to the same data, the second wave, which has phase angle of -003° and an amplitude of 0.997707, is detected with a phase angle of -003° and an amplitude of 0.946315 and the S2 wave is detected with a phase angle of -170° and an amplitude of 0.052728. This demonstrates that HiCum is able to detect a wave phase difference to a high degree of precision when the time period can be clearly defined.

5.2 A second scenario exploring the effect of noise and quantity of data on the quality of results.

This was aimed at determining how the accuracy of detection of a waveform is affected by both the size of the noise to signal ratio, k, and the number of readings taken, N.
The values of k used were 0, 1, 10, 100 and 1000 (0 = no noise). The time periods were 10, 100 and 1000 days. The phase and amplitude of the S2 wave for each scenario is given in the table below.

	N	10 days		100 days		1000 days	
k		Phase	Amplitude	Phase	Amplitude	Phase	Amplitude
0		-173°	0.999802	-173°	0.9998	-173°	0.999793
1		-174°	0.998864	-173°	1.00031	-173°	0.999956
10		-170°	1.00116	-173°	0.990286	-173°	0.998895
100		-145°	1.13387	-169°	0.906448	-174°	0.990887
1000		-094°	5.45362	-088°	0.59966	-179°	0.918826

Table1 A table showing how the ability to detect a wave's amplitude is affected by the noise and the number of readings taken.

As is expected, we can see from Table 1 that as the noise to signal ratio increases, the ability of HiCum to detect the signal diminishes. However, we can also see that if the number of readings taken is increased, then HiCum is able to detect the signal in a highly noisy environment. This is a direct result of the methodology being based on the summation of repeated weak periodic signals, resulting in a strongly identifiable signal.

6 Example of information from HiCum using field data

The following section shows an example of the analysis of data records from a super conducting gravimeter by van Ruymbeke et al (2001). Using the HiCum method, a constant length time period M2-wave was selected. The fundamental sine wave was then removed and the residual data checked for any non-linearity or harmonics present.

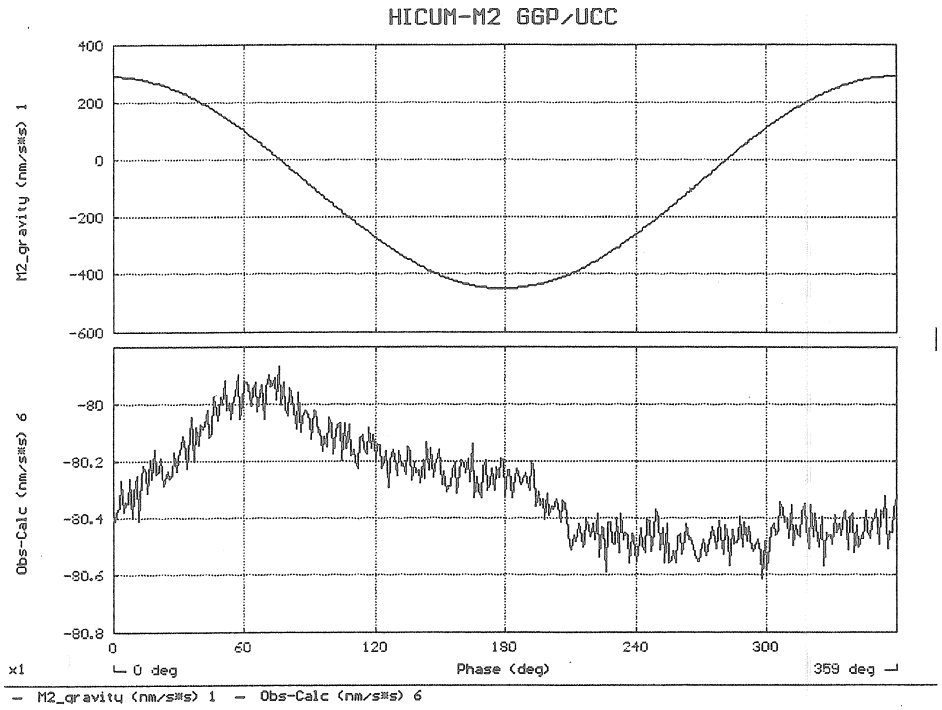

Fig. 4. Top: An amplitude-phase plot of the HiCum-M2 for the gravity versus the HiCum-M2 for the theoretical earth tide.
Bottom: The same plot with the sinusoidal trend removed and a more sensitive scale on the y-axis

In order to determine the exact nature of the signal the detected signal is plotted against M2 and from the top graph in Figure 4 we can see near perfect linearity with an amplitude of around 350 nm/s². In the lower graph the pure sinusoidal signal is then removed and the sensitivity of the scale is increased to reveal the non-linear behaviour of M2 component with a residue of less than 0.3nm/s². This residue represents a small lag between the two signals, and a non-linear behaviour with an amplitude of lower than 30 nanoGal, i.e. close to 0.1% of the amplitude as recorded by the gravimeter. This detection of non-linear hysteresis on raw data would not be possible with Spectrum Analysis and so demonstrates the usefulness HiCum in situations where the time period is known. The high level of precision on a weak signal was possible, because records were taken repeatedly over years and the results from the same time period each day were added, stacked, resulting in an averaging effect producing a detailed picture of the daily variations.

7 Using HiCum

μDAS Grapher can be downloaded from the internet. Below is a detailed description of how μDAS Grapher was used to prove the accuracy of the HiCum method for analysing the type of data expected from the Gravitational Balance GB02, which is currently under development at the Observatoire Royal de Belgique. As above a series of known cosine waves and noise signals were computer generated. In order to simulate the signature of

the Gravitational Balance GB02, the selected cosines were of time periods 720s and 750s representing the oscillations of the masses and the eccentric cam respectively. Noise signals were also generated one with a noise to signal ratio of 1:1 and the other 10:1. The signals were constructed from 3000 data points created at 6s time intervals representing 18000s or 5h of data. This data was then transferred to µDAS Grapher.
NB The files should be opened in MGR with /ic to interpret all commas as decimal points and /i:s to put a time base on the data, each command must be separated by a space.

Once the file had been loaded into µDAS Grapher The data function was used to mix the signals using the formula option. *Select Alt A then F8, you will then be prompted for your required formula.* Figure 3 shows the various scenarios that were created. *To add channels simply enter the number or the letter of the channel as a sum e.g. 1+2. If you need to enter a numerical function then the number should be enclosed in brackets <> to distinguish it from a channel number e.g. 3.<0.5> multiplies channel 3 by 0.5.*

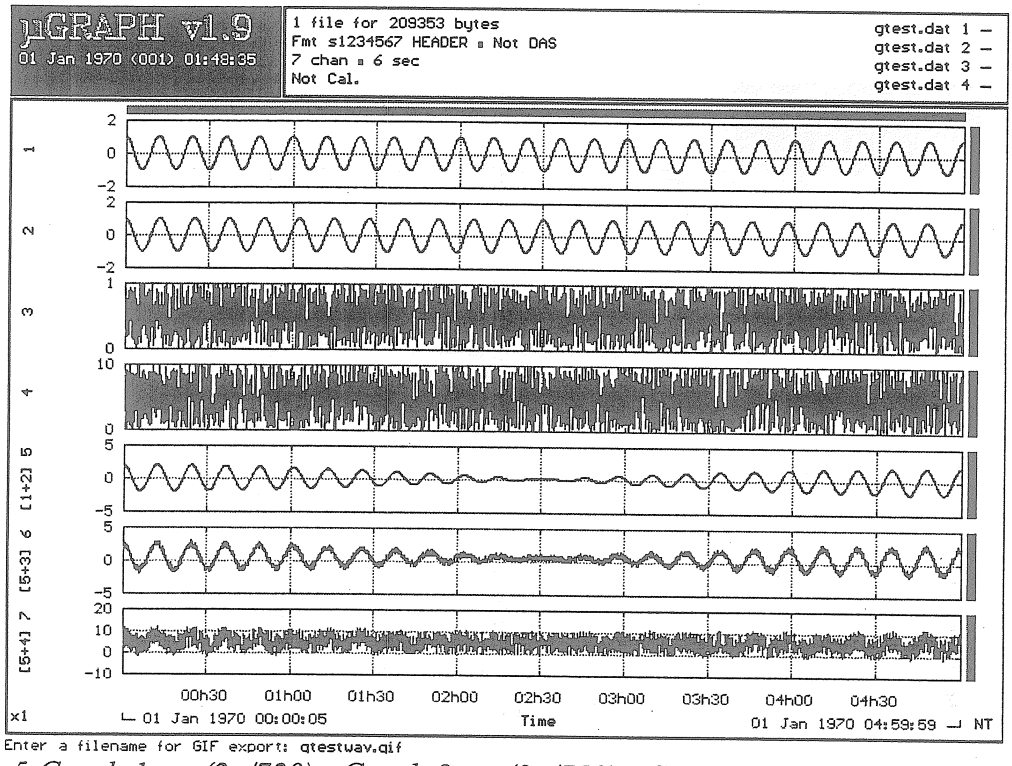

Figure5 Graph 1 cos(2π/720)t, Graph 2 cos(2π/750)t, Graph3 noise 0-1, Graph 4 noise 0-10, Graph 5 the addition of the two cosine waves, Graph 6 two cosine waves with noise 0-1, Graph 7 two cosine waves with noise 0-10.

The signals were then analysed using HiCum to see if the individual original waveforms could be detected. *To do this you need to enter shift F8 and you will be prompted to enter the time period for the first wave Our first wave had a time period of 720s but we needed to enter 120 (720/6) since our choice for the generated wave had been data at 6s intervals.* When the time period 720s is applied HiCum should be able to detect that wave and pick up little of the second wave, conversely when the time period 750s is analysed,

the second wave should be detected and little from the first wave. The results are shown below.

Figure 6 is a graphical demonstration of how the various scenarios shown in figure 5 compare with a wave of time period 720s. For each of the synthetic signals we can see the summation of the histograms created from the signal when it has been divided into lengths of 720s and how this compares with a wave of time period 720s. As expected there is an exact correlation for the 720s wave with no noise (graph 1), we can also see a good correlation when the waves are mixed and noise is added (graphs 5-7). *To obtain the comparisons press F7 the third strike gives the 1st harmonic, as shown below in figure 6. The first strike will give the mean value, the second the linear regression, the fourth the 2nd harmonic, the fifth the 3rd harmonic and the sixth the 4th harmonic a further strike brings you back to nothing being superimposed, no examples of these options are given in this text.*

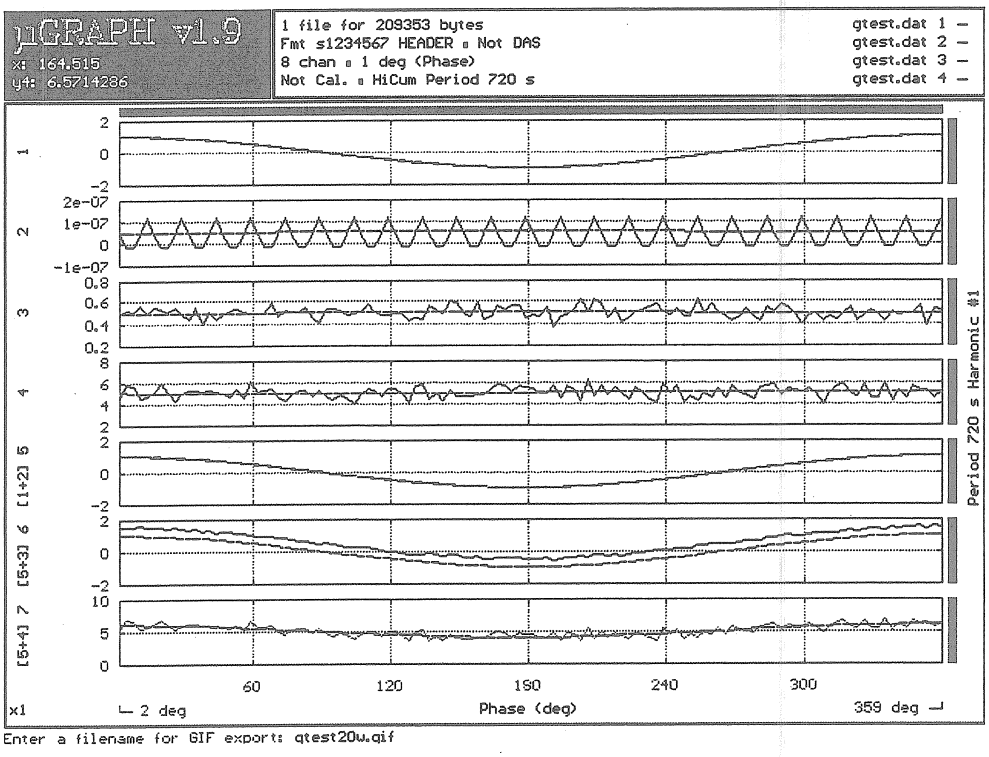

Figure 6 A comparison of a wave of period 720s with the scenarios shown in figure 5.

Figure 7 gives the numerical comparisons of phase and amplitude for the various signals. *To obtain this information press F2 twice, pressing Esc will remove the data.* From figure 7 we can see that the original wave has a phase of –001° and this is clearly detected from a situation where the two signals are mixed and also when the signals are mixed with a signal, having a noise to signal ratio of 1:1. On mixing the signals with a noise to signal ratio of 10:1 the accuracy is reduced giving a phase of –003°.

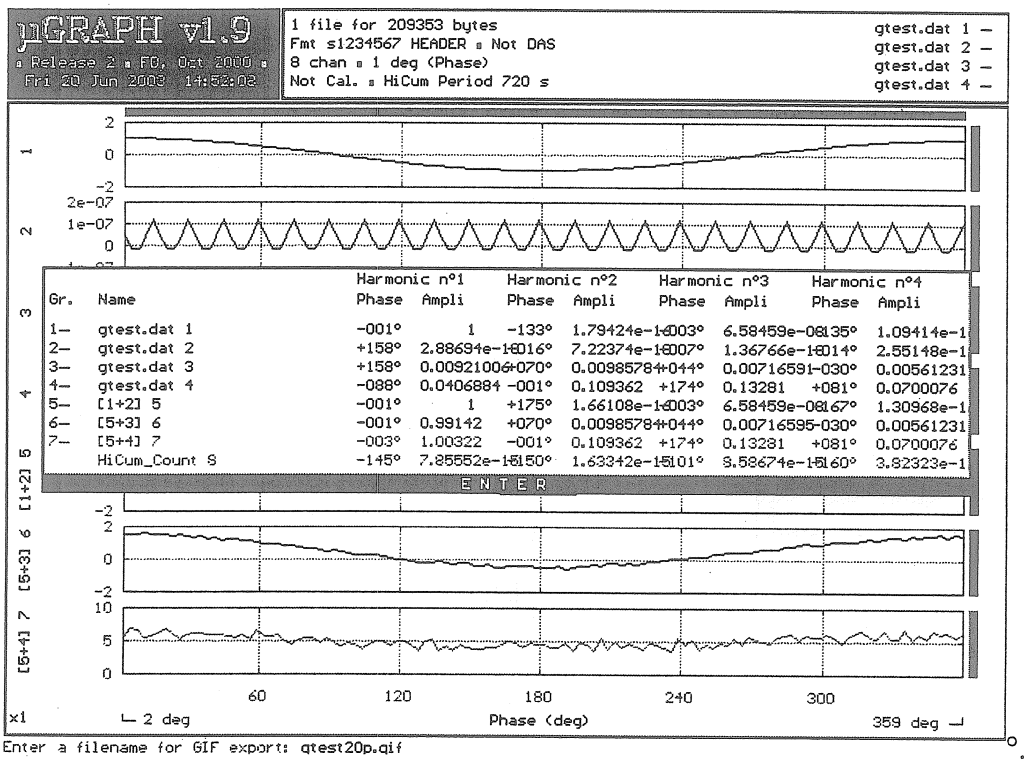

Figure 7 A numerical analysis of the scenarios shown in figure 6

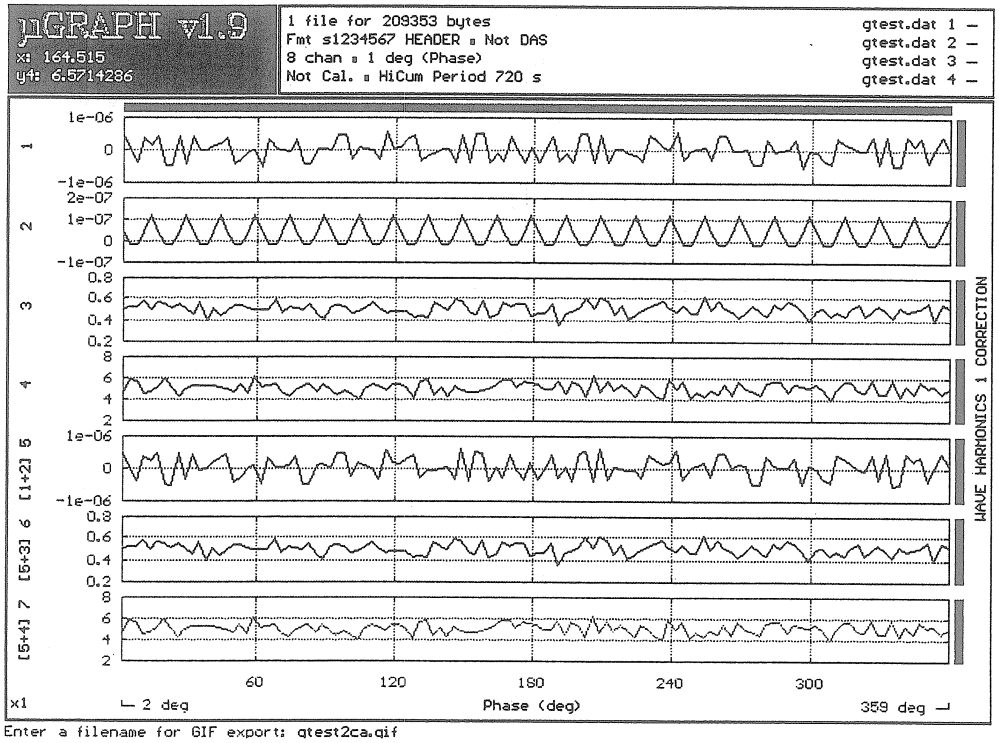

Figure 8 The residual signals for each scenario once a signal of time period 720s has been removed.

Using HiCum the fundamental wave can be subtracted from each of the scenarios. *This is done by pressing enter, when prompted to, after typing F7 the required number of times.* The residual signal is then detected, this is shown in figure 8. As might be expected the levels of these residuals vary enormously, and is clearly demonstrated by the different scales required for the y-axis. *Before analysing the data for the second time period this data should be saved by pressing F1. To save any images created in μDAS Grapher you first need to change the image from colour to black with a white background by pressing F9 twice. Then to save press shift F1 and give your file a title with a gif extension e.g. spring.gif*

Figures 9,10 and 11 show the corresponding results from entering a time period of 750s.

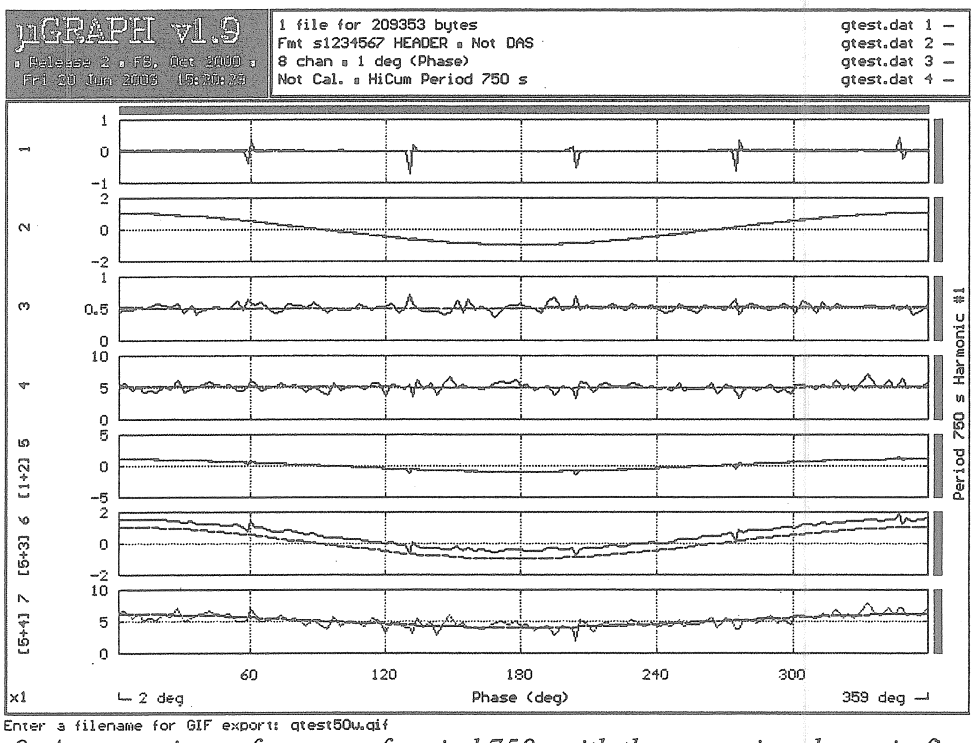

Figure 9 A comparison of a wave of period 750s with the scenarios shown in figure 5.

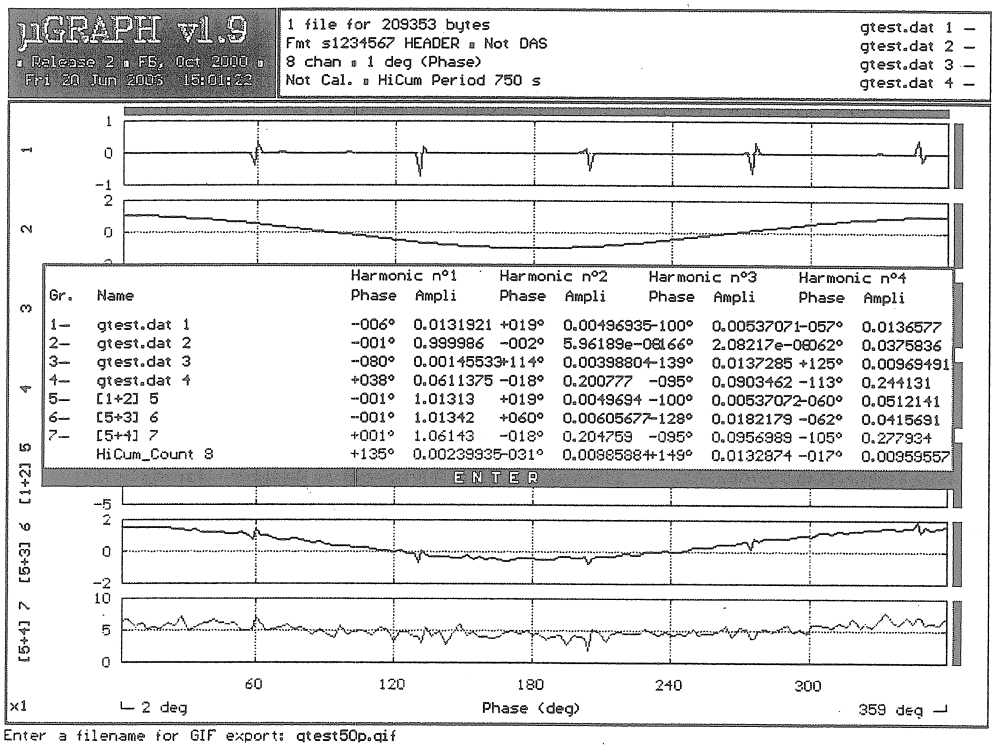

Figure 10 A numerical analysis of the scenarios shown in figure 9.

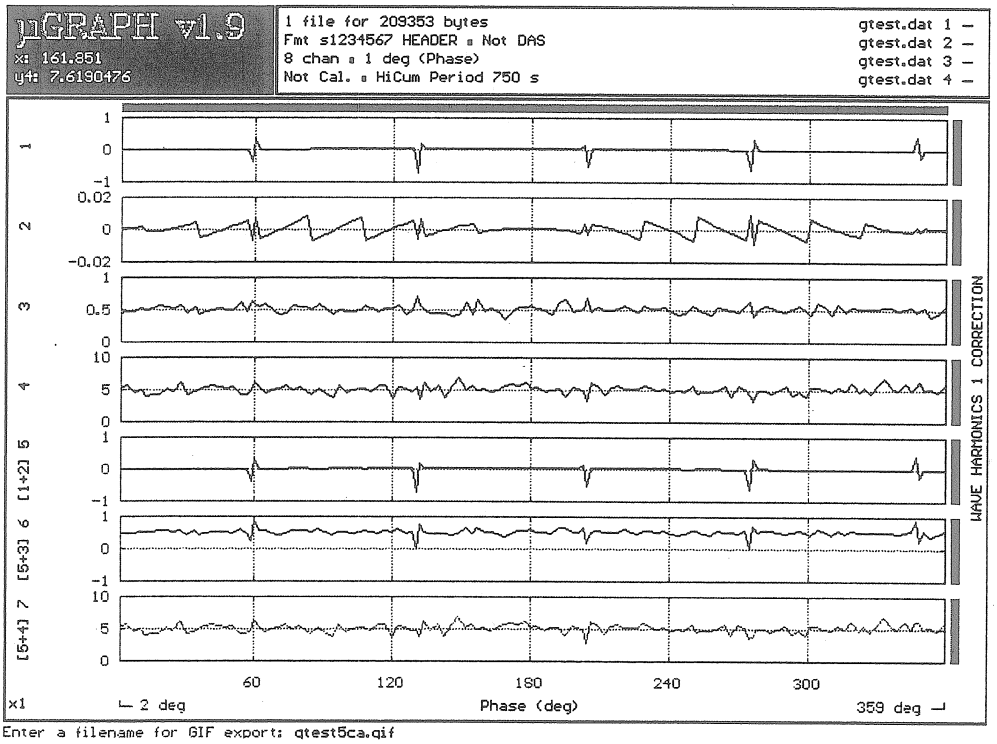

Figure 11 The residual signals for each scenario once a signal of time period 750s has been removed.

From Figure 9 we can see that once again the selected wave has been detected with a noise level of 1:1. Even with a noise level of 10:1 the selected wave is detectable. From

this example we can see that with only 3000 data points two signals have been accurately detected from data containing a mixture of these signals and noise. In addition the residual values have been determined.

8 Conclusion

The use of computer-generated signals has demonstrated the power of the HiCum method in detecting signals in a noisy environment when the time period is known. The accuracy of the method has also been shown to be extremely powerful in the analysis of field data. HiCum is a successful tool because a weak signal has been recorded repeatedly and its cumulative result produces the equivalent of a strong signal with a wealth of detailed information. HiCum has been developed to analyse data from the EDAS system but is applicable to any situation where numerous readings can be taken during each cycle and over several cycles.

Bibliography

Van Ruymbeke M., Beauducel Fr., Somerhausen A. , 2001: The Environmental Data Acquisition System (EDAS) developed at the Royal Observatory of Belgium.
Journal of the Geodetic Society of Japan, 47, 1, 41-46

Emter D., Zürn W., Schick R., Lombardo G., 1986: Search for Tidal Effects on Volcanic Activities at Mt. Etna and Stromboli.
Proc. Tenth Int. Symp. on Earth Tides, Madrid, September 23-27, 1985. R.Vieira ed., Consejo Superior Investigaciones Cientificas, Madrid, 765-774

Bartels J, 1938: Random Fluctuations, Persistence and Quasi-persistence in Geophysical and Cosmical periodicities.
Terr. Magn. Atmos. Electricity, 40 , 1, 60

Zürn W., Rydelek P.A., 1994: Revisiting the phasor-walkout method for detailed investigation of Harmonic Signals in Time Series.
Surveys in Geophysics, 15, 409-431

Search for the Gravitational Absorption Effect Using Spring and Super-conducting Gravimeters during the Total Solar Eclipse of August 11, 1999

Michel van Ruymbeke [1], Liu Shaoming [2], Lalu Mansinha [3] & Bruno Meurers[4]

1) Observatoire Royal de Belgique, 3 Ave. Circulaire, 1180 Bruxelles, Belgium.
2) Institute of Seismology, China Seismological Bureau, Xiaohongshan, Wuhan 430071, China
3) Department of Earth Sciences, the University of Western Ontario, London, Canada N6A 5B7.
4) Institute of Meteorology and Geophysics, Hohe Warte, 38, A-1190 Vienna, Austria.

Abstract

In this paper we analyse the gravimetric records obtained with tidal instruments, during the solar eclipse on August 11, 1999, when the shadow crossed Europe.

Measurements recorded with spring and super-conducting gravimeters set up in Annelles, Uccle, Walferdange and Bondy are discussed.

Comparisons between super-conducting gravimeters and spring gravimeters are made, in order to fix the limits of the magnitude of abnormal effects in relation to the possibility of a shielding effect by the Moon on the Sun's gravitational attraction. The results from the LCR and Askania gravimeters will also be discussed in the paper.

Our conclusions are that significant effects during an eclipse, if indeed they do exist, may be below the noise level of the gravimeters which is $\pm 1 nm/s^2$ ($0.1 \mu Gal$) for super-conducting gravimeters.

Our findings confirm that in these situations both spring and super-conducting gravimeters are working at the limits of their precision, with a risk that abnormal environmental features induced by the eclipse could significantly modify the signals.

Keyword: *gravity, gravitational shield, gravimeter, solar eclipse, Earth-tide*

1. Introduction

An interest for gravity measurements during an eclipse by Tomaschek (1955) arose from the experiments and hypothesis of Majorana (1920) on gravitational absorption, often referred to as the *Majorana effect,* or, *gravitational shielding*. The validity of Majorana's hypothesis has been questioned by Russell (1921). Tomaschek's experiment was followed by gravimeter experiments during solar eclipses in the early sixties by Slichter, Caputo and Hager (1965) and many others. A comprehensive review of gravimetric and barometric observations during eclipses has been given by Sun (1995).

The failure to observe any significant change in g during eclipses in the early nineteen-sixties resulted in a hiatus of similar experiments for a period of about 30 years.

Recently Ducarme, Sun, d'Oreye, van Ruymbeke and Mena Jara (1999) reported on gravimeter and microbarometer observations during the 1991 eclipse in Mexico.

This was followed by a collaborative campaign for the November 3rd, 1994 Eclipse (De Freitas et al. 1995).

On March 9th, 1997, in China, there occurred a total eclipse of sun. During the eclipse, in Moho, Heilongjiang province, China, which was in the shadow centre of the eclipse, Wang *et al.* (2000) carried out a series of gravity measurements. Their purpose was to detect the possible effect of gravitational shielding during a total eclipse. The observation instrument they used was a LaCoste-Romberg D gravimeter (L&RD-122). After all necessary corrections, the residue shows two significant gravity decreases. One occurred during the first contact with amplitude of 5.3±1.4μgal. Another occurred during the last contact with amplitude of 6.8±1.4μgal. Wang et al suggest that these two gravity changes may result from some extraordinary phenomenon associated with gravity, such as the possible shielding effect by the moon on the gravitational force of the sun. However, they also stated that more high precision measurements should be carried out in the future, to further study this phenomenon, especially during solar eclipse.

The main goal of this paper is to compare, for the eclipse of August, 11th, 1999, measurements recorded by spring gravimeters and by super-conducting gravimeters in order to determine the reality of the effects recorded in China.

2. Spring and super-conducting gravimeters monitoring

For events with few hours duration, spring gravimeters can resolve significant changes in g of $10^{-8}ms^{-2}$ (1μGal). The super-conducting gravimeters (SGs) can resolve changes of 10^{-9} ms^{-2} (0.1μGal). So SGs are more suitable for observing the possibility of effects like shielding, which may be extremely small, if indeed they exist. However, because the SGs are not as easily transportable as spring gravimeters, almost all eclipse experiments are conducted with transportable spring gravimeters.

3. The August 11th, 1999 Eclipse monitoring with super-conducting gravimeters

The results of a collaborative observation campaign of gravimetric monitoring observed during the eclipse on August 11, 1999 over Europe (fig.1) are given below.

On August 11, 1999 a total eclipse occurred in Europe. The shadow path passed near to four SG stations at Uccles and Membach, (Belgium), Strasbourg, (France) and Vienna, (Austria). It provided a unique opportunity to search for the gravitational shielding effect with the more sensitive SGs.

Lalu *et al.* (2001) described the gravity measurement, processed the data and discussed the results. After tides and air pressure corrections, the results of the four SG stations show that the super-conducting gravimeter has the same limitation of noise as the transportable spring gravimeters for this type of experiment and there is no perceptible change in g above the ambient noise level during the totality. The records from the Vienna SG will be discussed in order to fix the limit of precision in detecting existing phenomena with this high quality probe.

The SG GWR C025 in the Vienna station, which is located at the NW margin of Vienna, has been recording gravity and air pressure continuously since 1995.
This station lies very close to the main path of the eclipse in Europe on August 11, 1999. Its sun obscuration was 99% during that eclipse. The first and last contacts for the eclipse at the Vienna station were 9:23.5 and 12:08.6 respectively, totality was at 10:46.2.

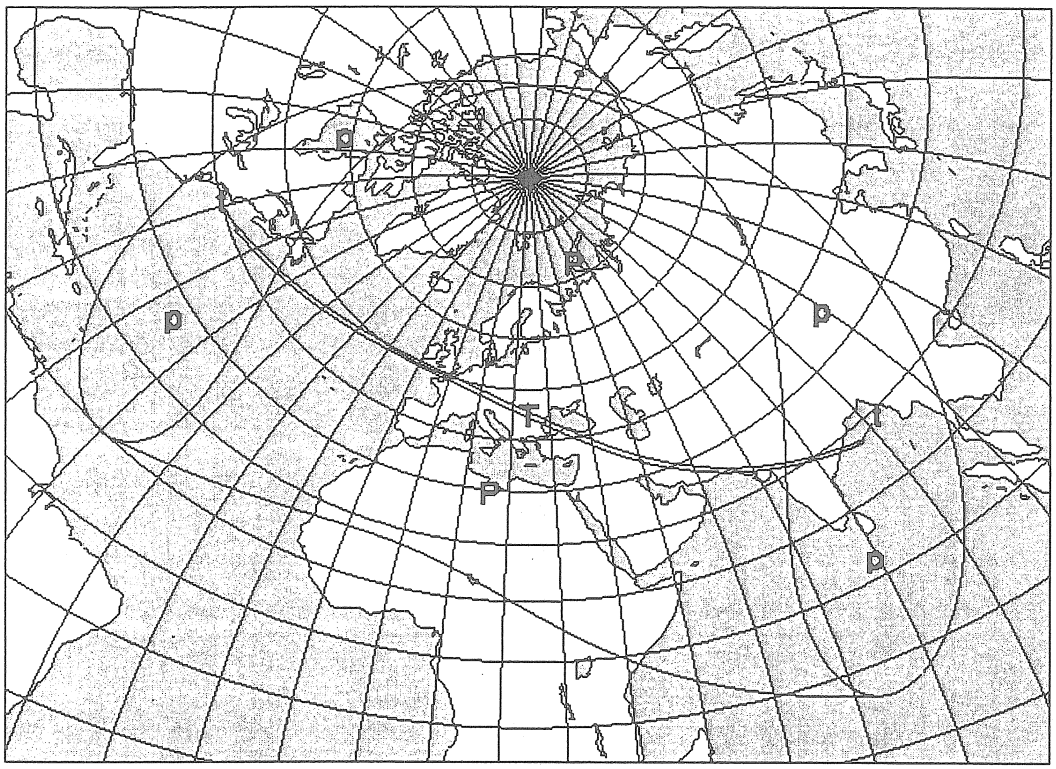

Figure 1: Shadow zones for August 11, 1999 Solar Eclipse. The Totality zone (T) crosses Europe; The P zones are penumbra areas.

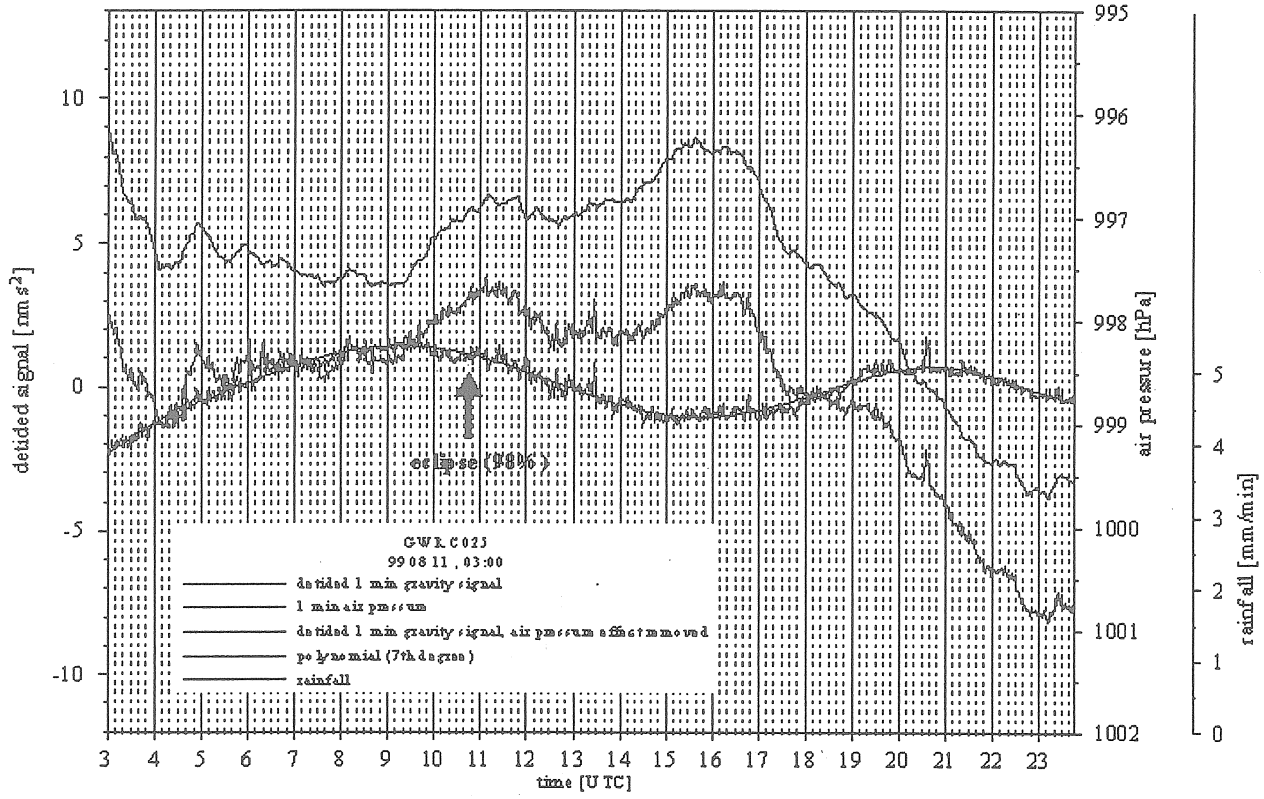

Fig. 2: Gravity and air pressure during the eclipse on August 11, 1999, in Vienna observed with SG C025. The upper curve shows the pressure changes, the middle curve shows the gravity residues and the lower curve shows the gravity residues corrected for pressure. The first and last contacts for the eclipse at Vienna station are 9:23.5 and 12:8.6 respectively, totality was at 10:46.2.

Meurers processed the gravity and air pressure data of the Vienna station during that eclipse. The results he obtained are showed in Fig.2. All curves have been filtered, so the sample interval is 1 min. The upper curve shows the air pressure changes. The middle curve shows gravity changes after tidal correction. There is a good correlation between these two curves. After the air pressure effect was subtracted from the gravity effect, by applying a constant admittance factor of $-3.53 nms^{-2}/hPa$, the gravity residual became smooth, which is shown by the lower curve. The gravity changes remaining in the residual signal, obtained after application of the corrections of tides and atmospheric pressure effects, is lower than 0.4 μGal for periodicities comparable to semi-diurnal process. For the periodicity of the eclipse modulation, oscillation amplitudes are less than 0.1 μgal.

4. The August 11th, 1999 Eclipse integrated monitoring with spring and super-conducting gravimeters

In order to monitor the possible shielding effect of the Sun's attraction during a Solar eclipse, the Royal Observatory of Belgium set up a network of gravimeters with LCR, Askania and SG for the eclipse of August 11th, 1999. It was centred on the village of Annelles in northern France, within the zone of totality. Gravity changes were observed in parallel with the air pressure, temperature, luminosity and rainfall (van Ruymbeke,M. & al.,2001). Among the stations within the network were Annelles, Uccle ,Walferdang and Bondy stations.

The results from each of these stations are discussed below.

4.1 The result from Annelles station

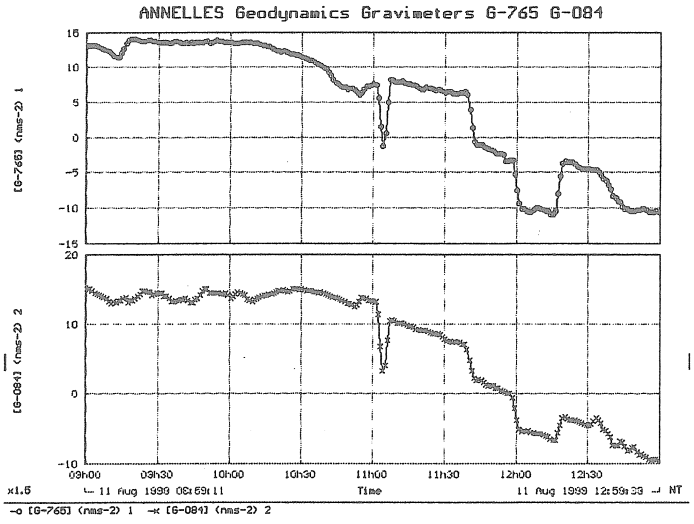

Fig.3: Gravity changes from 3:00 to 12:30 on August 11, 1999 at Annelles station. The two curves show the de-tided records of gravity changes for the gravimeters Geodynamics G-765 (top) and G-084 (bottom). The first and last contacts at Annelles station are about 9:00 and 12:00 respectively, with totality at 10:30

Two Geodynamic gravimeters were used to carry out the gravity measurement during the 11 August 1999 eclipse at the Annelles station. Fig.3 shows the gravity changes during the eclipse from 9:00 to 13:00. The first and last contacts at Annelles station are about 9:00 and 12:00 respectively, totality was at 10:30.The gravity curves

are obtained after tides and air pressure correction. All the data was filtered by 10 min. There is a very good correlation between these two curves, with the overall tendency, shown by the two curves, being a decrease. No abnormal gravity that was beyond 0.2uGal for SG and 1 uGal for LCR were detected. So no shielding effect beyond noise level was found to exist.

4.2 The result from the Uccle station

At the Uccle station a Super Conducting Gravimeter and a LCR gravimeter were use to conduct the gravity measurement. Fig.4 shows the gravity change from 9:00 to13:00, 11 August 1999. *The first and last contacts at Uccle station are about 9:00 and 12:00 respectively, with totality at10:30.* The gravity changes are air-pressure-corrected and tides-corrected. All data was filtered by 2 min. In Fig.4, the first curve shows the gravity change recorded by the SG and the second one shows the gravity change recorded by the LCR gravimeter. The overall tendency of the first curve is a decrease. The overall tendency of the second curve is a rise. There is no obvious correlation between the two curves. No common abnormal gravity change that is beyond 1μGal for the SG and the LCR gravimeter is detected. So again no visible shielding effects beyond noise level were found to exist during the eclipse.

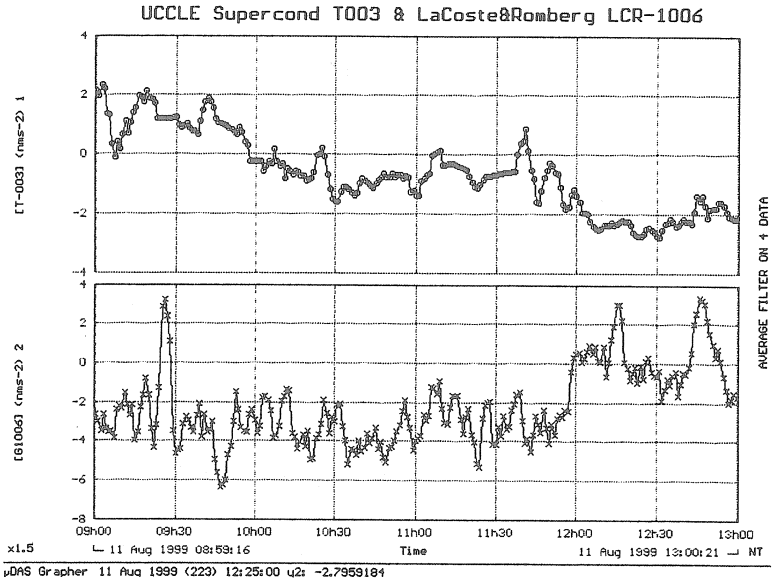

Fig.4 : Gravity changes from 9:00 to 13:00 on August 11,1999 at Uccles station. The two curves show the de-tided records of gravity changes for the gravimeters Super Conducting T-003 (top) and LaCoste&Romberg 1006 (bottom). The first and last contacts at Uccles station are about 9:00 and 12:00 respectively, with totality at 10:30

4.3 the result from Walferdange station

Two Askania gravimeters are used to record the gravity changes at the Walferdange Station during the eclipse on August 11, 1999. Fig. 5 shows the gravity changes recorded by the two Askania gravimeters from 9:30 to 12:22. The first and last

contacts at the Walferdange station are about 9:00and 12:22 respectively, with totality at 10:30.All data has been filtered by 2 min. The overall trends of the two curves are same. First they decrease and then they increase. There is no correlation between the detailed gravity changes in them. It seems that for this type of experiment, the precision of Askania gravimeter is about 3μGal. No common abnormal gravity change more than 3μGal can be seen in Fig 5 during the eclipse. So the results from the Walferdange station show that no shielding effects beyond noise level exist.

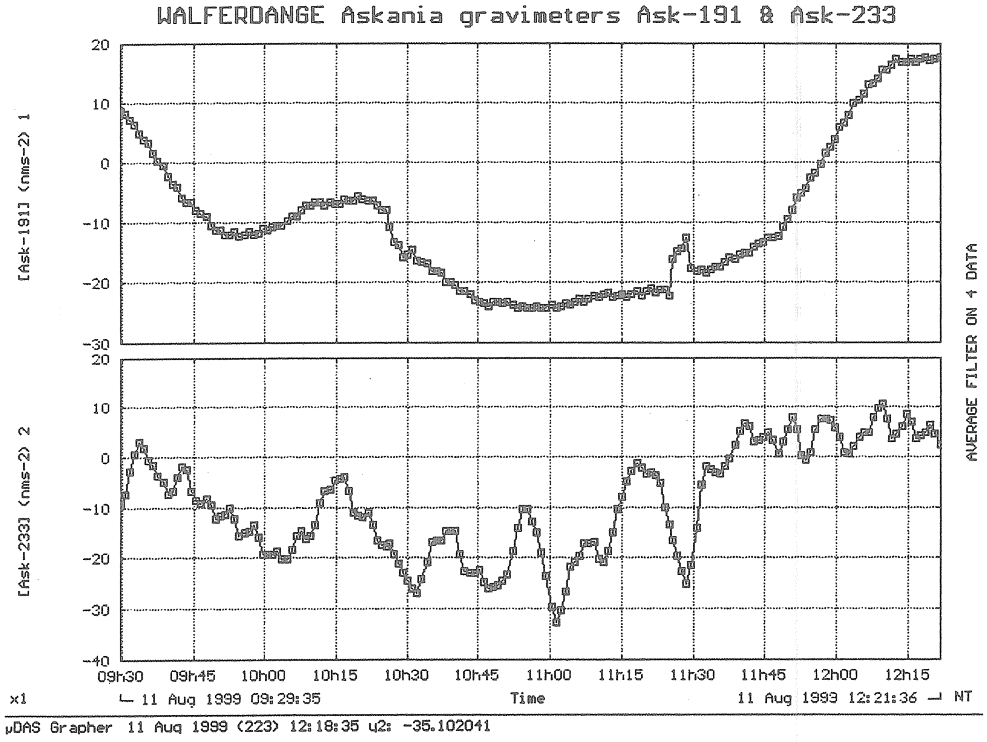

Fig.5: Gravity changes from 9:30 to 12:21 on August 11, 1999 at Walferdange Underground Laboratory of Geodynamics. The two curves show the de-tided records of gravity changes for the gravimeters Askania 191 (top) and Askania 233 (bottom). The first and last contacts at Walferdange station are about 9:00and 12:22 respectively, with totality at 10:30

4.4 the results from the Bondy station

Two LCR gravimeters were used to conduct the gravity measurements during the eclipse at the Bondy station. Fig.6 shows the gravity change from 9:21 to 13:00, 11 August 1999. The first and last contacts at Bondy station are about 9:00and 12:00 respectively, with totality at10:30. All data was filtered by 2 min. The overall tendency of the first curve is decrease. The shape of the second curve is slightly more complicated. At first it decreases, then it increases, then it decreases again, and at last it increases. In the second curve there is a gravity change about 2μGal which is beyond the noise level. As only one gravimeter recorded any gravity change that is beyond noise level, we do not think that the shielding effect has been observed. It is more likely that the abnormal gravity in the second curve is due to a manmade occurrence.

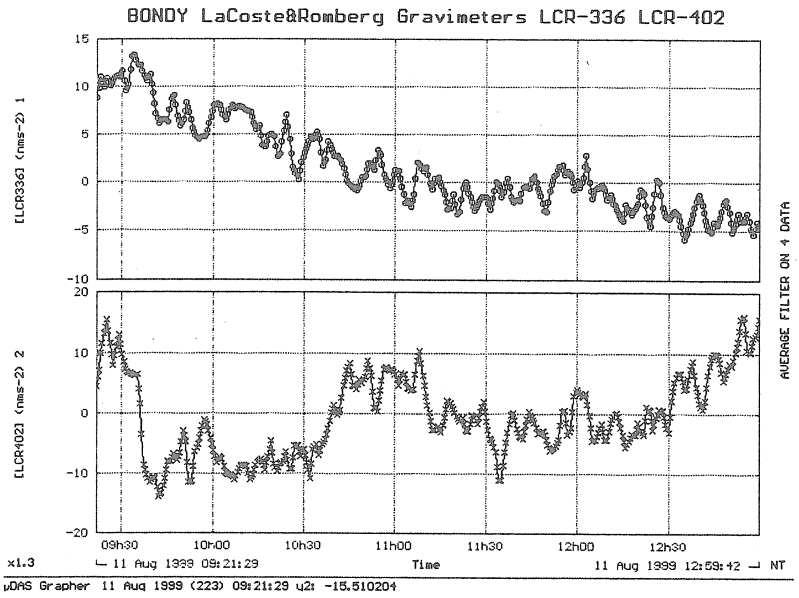

Fig.6: Gravity changes from 9:21 to 13:00 on August 11, 1999 at Bondy station. The two curves show the de-tided records of gravity changes for the gravimeters LaCoste&Romberg 336 (top) and LaCoste&Romberg 402 (bottom). The first and last contacts at Bondy station are about 9:00 and 12:00 respectively, with totality at 10:30.

5. Discussion about the magnitude of any possible shielding effect

According to Newton's Law of Universal Gravitation, the force made by the attraction of the Sun, F_s, acting on a mass, m, which is on the surface of the Earth, is given by

$$F_s = Gm\frac{M_s}{b^2} \qquad (1)$$

Where G is the gravitational constant, M_s is the Sun's mass and b is the distance from the sun to the mass. The gravitational attraction of the Earth acting on the mass is given by

$$F_e = Gm\frac{M_e}{a^2} \qquad (2)$$

where g is the acceleration due to gravity, G and m are the same as those in equation (1), M_e is the mass of the Earth and a is the radius of the Earth.

Let the constant, γ, be defined as:

$$\gamma = \frac{F_s}{F_e} \qquad (3)$$

Substituting equations (1) and (2) into equation (3), gives us

$$\gamma = \frac{M_s a^2}{M_e b^2} \qquad (4)$$

Taking the following approximate values:

$$M_s = 2\times10^{30}\,kg$$
$$M_e = 6\times10^{24}\,kg$$
$$a = 6.4\times10^{6}\,m$$
$$b = 150\times10^{9}\,m$$

we obtain a value for γ:

$$\gamma = 6\times10^{-4} \qquad (5)$$

Re-arranging equation (3) gives us:

$$F_s = \gamma g.$$

Taking a value of: g=9.8 m/s^2, gives us:

$$F_s = 0.6 Gal.$$

If the shielding effect observed by Wang *et al.* (2000), which is about $6\mu Gal$, is the case, its proportion to the attraction force of the Sun (F_s) is about 10^{-5}. With the current level of precision of modern observation techniques, this effect is large enough to be observed.

Such a shielding phenomenon would result in numerous effects, such as perturbations of the moon, the inequality of ocean and earth tides on sides facing and away from the sun, perturbation of satellite's orbits, etc.

Furthermore if a gravitational shielding effect is found to exist, then the question arises whether the Earth itself could act as a shield. For example would the force causing tides, due to the attraction of the moon, be less on the side of the Earth farthest from the moon, as a result of a shielding effect of the Earth itself? Of even more fundamental importance, is whether we would have to redefine the model for the computation of the Earth's gravitational field, to include a factor to represent the shielding effect of the Earth on its own gravitational field.

6. Conclusions

The results presented in this note, in common with most earlier eclipse experiments, show that there is no perceptible change in g, above the ambient noise level during totality, as recorded by spring gravimeters. At the Bondy station one spring gravimeter did not record abnormal gravity changes, but the other one did. This is a typical situation, showing the difficulties associated with working with spring gravimeters at the limit of their precision.

In Lalu *et al.* (2001), the records of four superconducting gravimeters permitted us to look for common signal shapes during the eclipse period. We are confident that a common signal pulse of amplitude of at least 2×10^{-9} ms^{-2}, if present, would have been detected. However, no such change was observed, so no change of g can be attributed to gravitational shielding from these results.

This contradicts the report by Wang. *et al.* (2000), who observed anomalous changes in *g* at first and last contact in an experiment during the eclipse in 1997 in China. The most likely explanation for the changes in gravimetric readings is an eclipse related effect. An effect probably induced by some electrical occurrence due to the special situation of night conditions occurring during the day.

Acknowledgements:

The authors are grateful to Pr. P.Pâquet, Director of the Royal Observatory of Belgium who provided the necessary support. We wish to thank the different Technical Institutes who helped to build the EDAS equipment for this project. We thank the European Commission for its support in the development of the EDAS concept. This experiment became a reality thanks to the support of Solvay S.A. and OCE Belgium. The authors would like to extend their gratitude to Ing. G.Berthault, for his help and support, as well as to Ing. D.Tassot for their support and logistics in Annelles. We cannot name all the participants who helped us throughout Europe in installing the network, but we remain indebted to them. We are also grateful for the scientific collaboration we had with Dr Sun He-Ping Dr B.Ducarme and Dr Nicolas d'Oreye de Lantremange. Thanks also to Rosamund Howard who proof read the text.

Bibliography

Chimonas, G. (1970): Internal gravity-wave motions induced in the Earth's atmosphere by a Solar eclipse. *J. Geophys. Res.*, 75, 5545-5551.

De Freitas, S.R.C., van Ruymbeke, M., Ducarme, B., Somerhausen, A., Mantovani, M.S. and Shukowsky, W. (1995): On gravity measurements related with the November 3, 1994 Solar Eclipse in Brazil. (Abstract) *IUGG XXI General Assembly*, Boulder.

Ducarme, B., Sun, H.P., d'Oreye, N.,van Ruymbeke, M. and Mena Jara, J. (1999): Interpretation of the Tidal Residuals during the July 11, 1991 Total Solar Eclipse, *Journal of Geodesy, 73, 53-57*

Mansinha L., Ducarme B., Hinderer J., Meurers B., van Ruymbeke M. (2001): Search for the Gravitational absorption effect using superconducting gravimeters during the eclipse of August 11,1999. *Journal of the Geodetic Society of Japan, 47, 1, 387-391.*

Majorana, Q. (1920): On gravitation: theoretical and experimental researches. *Philosophical Magazine* 39 488 - 504.
Russell, H.N. (1921) On Majorana's theory of Gravitation. *Astrophysical Journal* 54 334-346.

Slichter, L.B., Caputo, M., and Hager, C.L. (1965): An experiment concerning gravitational shielding. *J. Geophys. Res.* 70 1541-1551.

Sun, He-Ping (1995) Preliminary Report on Study of the Atmospheric Pressure Variations and its Influence on Gravity Observations During the Solar Eclipses. *Royal Observatory of Belgium, Brussels. 92pp.*

Sun, He-Ping (1995): S., Static Deformation and Gravity Changes at the Earth's Surface due to the Atmospheric Pressure, Dissertation Doctorale, *Royal Observatory of Belgium, Brussels.*

Tomaschek, R., (1955): Tidal gravity measurements in the Shetlands: Effect of the total eclipse of June 30, 1954. *Nature*, 175, 937-939.

van Ruymbeke,M., Somerhausen, A. & Mansinha L. (2001): Climatic Effects Measured During the Eclipse of August 11,1999. *Journal of the Geodetic Society of Japan. 47, 1, 380-386.*

van Ruymbeke, M., Beauducel F., Somerhausen, A., The Environmental Data Acquisition System (EDAS) developed at the Royal Observatory of Belgium. *Journal of the Geodetic Society of Japan. 47, 1, 40-46.*

Wang Qianshen., Yang Xinshe, .Wu Chuanzhen, Guo Honggang, Liu Hongchen and Hua Changchai (2000): Precise measurement of gravity variation during a total solar eclipse. *Physical Review D, 62, 4, 041101*®.

Search for the Translational Triplet of the Earth's Solid Inner Core by SG Observations at GGP Stations

He-Ping Sun[1], Jian-Qiao Xu[1], Bernard Ducarme[2]

1)Key Laboratory of Geodynamic Geodesy, Institute of Geodesy and Geophysics, Chinese Academy of Sciences, Wuhan, China
2)Belgium National Fund for Scientific Research, Royal Observatory of Belgium, Brussels, Belgium

Abstract A very large data set of 21 high precision tidal gravity observation series recorded with superconducting gravimeters (SG) at 14 stations in the Global Geodynamics Project (GGP) network are used to search for the translational triplet of the Earth's solid inner core (Slichter mode). The original observations at each station are pre-processed carefully at the International Centre for Earth Tides with an identical remove-restore technique. The time series of the tidal gravity residuals are obtained after subtracting synthetic signals and pressure influence. The power spectral densities for 8 long-term and 13 short-term series are estimated using 12000h Parzen window function based on the FFF technique, then the product spectral densities are calculated using a stacking technique. In order to detect effectively any weak geodynamical signals from the interior of the Earth, the remaining pressure effect is further removed. The final results show several significant common spectral peaks but not where previous studies had recently located the Slichter triplet. Most of the peaks probably correspond to the five- and six-diurnal non linear tides and it is probably a mere coincidence if the periods determined theoretically for the Slichter modes, fit three of the common peaks. However, we shall not be able to confirm them as the spectral peaks will be obscured by the non-linear tides generated either by oceanic effects or instrumental non-linearities. The study shows also that the detection of the dynamic effects of the solid inner core motion and other general core modes is a very complicated task. We estimate the detection limit on the gravity signals induced by the core mode to be 0.7 nGal level when the global SG observations are stacked simultaneously. The further investigation depends on the establishment of an acceptable theoretical model and the accumulation of long-term global SG data.

1 Introduction

The translational oscillations of the Earth's solid inner core, which include the equatorial prograde, axial and equatorial retrograde translations near the centre of the Earth, are the fundamental free modes of the Earth that usually called the Slichter triplet or Slichter mode if one use a non-rotate Earth model [*Slichter,* 1961]. The predominant components of these eigenmodes are degree 1 spheroidal displacement vectors (called also the eigenvectors). However other kind of spheroidal and toroidal displacements (with same order but different degree) are coupled with them due to Earth's ellipticity and rotation [*Smith,*1974]. By using a generalized spherical harmonic expansion technique, the translational triplet was theoretically studied by *Smith* [1976] and the eigenvectors were expressed as sum of 1st degree spheroidal and 2nd degree toroidal displacement vectors σ_1^m and τ_2^m (m=-1, 0 and 1). They were expected as 4.916h, 4.441h and 4.055h for equatorial prograde, axial and equatorial retrograde translational components when adopting a DG597 Earth model. This study showed that the influence of stratification in fluid outer core and elastic property of the solid inner core on eigenperiods to be significant. To overcome the uncertainty due to the convergence of the generalized spherical harmonic expansion, the theoretical studies were developed using a finite element technique based on so-called subseimic approximation [*Smylie and Rochester,* 1981] and a variation approach [*Smylie et al.* 1992a, 1992b]. As a result, the eigenperiods of the Slichter modes were predicted as 3.581h, 3.766h and 4.015h for Earth's model CORE11 and 2.603h, 2.702h and 2.824h for model 1066A. However in their computation, the Brunt-Väisälä frequency, describing the stability of fluid stratification, is taken a constant in whole fluid outer core. This hypothesis may be not obviously reasonable and may lead to

some discrepancies in the numerical results. On the other hand the theoretical studies of *Smith* [1976] and *Crossley et al.* [1999] indicated that the magnitudes of gravity variation, due to core modes, may be at one nGal level only which falls inside the SG precision range [*Richter,* 1987]. The inertial waves induced by Earth's fluid outer core were studied by *Aldridge and Lumb* [1987], the possible discovery of these inertial waves using SG spectra at Brussels were investigated by *Melchior and Ducarme* [1986].

The modern SG manufactured by GWR has many advantages over a spring gravimeter, such as high-sensitivity, high-sampling rates, high-precision (10^{-12} *g*), long term stability and wide dynamics range [*Warburton,* 1985; *Goodkind,* 1991; *Crossley et al.,* 1999; *Ducarme and Sun,* 2001]. SGs provide us with an important tool for the detection of super-weak signals arising from dynamic behaviours in the Earth's deep interior. The International Centre for Earth Tides (ICET) has been collecting the SG data for more than 20 years and is also the data centre for the Global Geodynamics Project (GGP) network since 1997 [*Ducarme et al.,* 2002]. The global data set is now equivalent to more than 100 years of observations. By using these data, we hope to study the behaviours of the Earth's interior dynamics [*Ducarme and Sun,* 2001; *Sun et al.,* 2002a]. Based on the eigen-parameters of the Earth's resonance at certain periods, some significant constraints on physical properties can be obtained, such as density or viscosity of the Earth's deep interior [*Smylie,* 1992a; *Smylie,* 1999; *Smylie and McMillan,* 2000].

Past studies have shown that it is difficult to detect experimentally general core modes, including the Slichter modes for the following reasons: (1) there is no well-accepted theoretical set of eigenfrequencies due to our imperfect knowledge of core properties, such as density, (2) gravity signals from the core are relatively weak and (3) ground-based gravity observations are heavily contaminated by some known and unknown systematic background noise. In order to overcome the difficulties, the stacking technique for the SG data from various stations may be the most effective way to enhance common harmonic signals.

The first multi-station experiment was done by *Cummins et al.* [1991] based on stacking the IDA data from the LaCoste-Romberg spring gravimeters; no core modes signals could be identified clearly due to the poor sensitivity of the instruments. Four long-term SG data sets from Europe stations were stacked by *Smylie et al.* [1993a], who claimed that three weak resonance signals with central periods as 3.5820h, 3.7665h and 4.0148h could be identified. These periods were in agreement with those computed theoretically using the sub-seismic approximation [*Smylie et al.,* 1992a]. Using SG observations at six globally distributed stations and a more sophisticated stacking technique, further claimed identification of the inner core translational triplet was obtained by *Courtier et al.* [2000]. However, when using SG observations at stations Strasbourg/France and Cantley/Canada, the observational studies of *Hinderer et al.* [1995] and *Jensen et al.* [1995] did not find the spectral peaks related to the Slichter triplet claimed by *Smylie et al.* [1993a, 1993b] in their product and cross-spectrum. They suggested the use of simultaneous long-term SG data distributed globally. Therefore the main purpose of present study is to search for the translational modes of the Earth's inner core using SG data from the GGP network.

2 Data Preparation

Twenty one SG time series with a total of 755,866 hourly values at 14 global distributed stations are used in this study. The observation series are divided into two groups, group 1 (G-I) for 8 long-term series and group 2 (G-II) for 13 short-term series in which most of them are starting from the GGP period. The station information including the names, observation periods, atmospheric gravity admittances and coefficients of long-term instrument drift are given in Table 1. The data sets used include 7 stations in Europe (Brussels, Membach, Metsahovi, Potsdam, Strasbourg, Vienne and Wetzell), 3 stations in Asia (Esashi, Matsushiro and Wuhan), 2 stations in

northern American (Boulder and Cantley) and 2 stations in southern hemisphere (Canberra and Syowa).

During data pre-processing, the original observations are pre-processed carefully at the International Centre for Earth Tides (ICET) with identical remove-restore technique. The same procedure is applied on one minute sampled data using T-Soft [*Vauterin,* 1998]. Anomalous signals such as spikes, steps and large-amplitude ascillations caused by large earthquakes are carefully removed, by an interactive procedure. Missing data due to short power interruption are interpolated using a synthetic tidal gravity model. A low-pass filter is used to decimate one minute sampled data into hourly observations. The gravimetric tidal parameters are determined with ETERNA3.4 software [*Wenzel,* 1998] using the high precision tide-generating potential developments with 1200 waves developed by *Tamura* [1987]. Gravity residuals are obtained by subtracting synthetic tidal gravity from hourly observations. The pressure admittances C ($nm \cdot s^{-2} \cdot hPa^{-1}$) (see Table 1) are determined by a regression technique between gravity residuals and station pressure. The instrument drift is simulated using a quadratic polynomial (see polynomial coefficients in Table 1).

As a matter of fact, the gravity residual series *Res(t)* can be expressed as

$$Res(t) = Obs(t) - \sum_k \delta_k \sum_{i=\alpha_k}^{\beta_k} A_i \cos(\omega_i t + \varphi_i + \Delta\varphi_k) - C \cdot Pr(t) - \sum_{i=0}^{2} a_i \cdot t^i, \quad (1)$$

where *Obs*(t) and *Pr*(t) are original tidal gravity records and station pressure, δ_k and $\Delta\varphi_k$ the amplitude factor and phase difference of the k^{th} tidal wave group to be determined, α_k and β_k the initial and final index of the k^{th} tidal wave group in tide-generating potential, A_i, ω_i and φ_i are theoretical amplitude, angular frequency and initial phase.

Table 1. SG gravity residual series used in the present study

Station	Observation Period	C	a_0	a_1	a_2
G-I					
Brussels1/Belgium	1982-06-02~1986-10-15	-3.428	5477.74	5.1615×10^{-3}	-2.27187×10^{-7}
Brussels2/Belgium	1986-11-15~2000-09-20	-3.428	8261.31	-4.3336×10^{-3}	3.95268×10^{-8}
Membach/Belgium	1995-08-04~2000-05-31	-3.428	-1068.06	8.6815×10^{-3}	-7.62658×10^{-8}
Potsdam/Germany	1992-06-30~1998-10-08	-3.500	42.6904	1.2907×10^{-2}	-1.25675×10^{-7}
Strasbourg/France	1987-07-11~1996-06-25	-3.000	-752.296	3.7677×10^{-2}	-3.09172×10^{-7}
Boulder/U.S.A.	1995-04-12~2001-03-29	-3.240	4100.57	1.2123×10^{-2}	-6.78259×10^{-8}
Wuhan/China	1988-11-17~1994-01-04	-3.840	-270.722	7.5364×10^{-3}	-4.17849×10^{-7}
Cantley/Canada	1989-11-07~1993-08-17	-3.000	-1416.08	-2.5717×10^{-1}	2.18132×10^{-6}
G-II					
Brussels/Belgium	1997-07-01~2000-09-21	-3.428	8065.87	1.4342×10^{-2}	-3.33212×10^{-8}
Boulder/U.S.A.	1997-07-01~1999-06-30	-3.240	4298.51	1.1964×10^{-2}	-1.44745×10^{-7}
Cantley/Canada	1997-07-01~1999-09-30	-3.000	-530.54	7.0119×10^{-3}	-3.58618×10^{-7}
Canberra/Australia	1997-07-01~1999-12-31	-3.002	3271.41	3.4538×10^{-3}	-6.42189×10^{-9}
Esashi/Japan	1997-07-01~1999-12-31	-3.145	3161.77	-3.0466×10^{-3}	2.58302×10^{-7}
Matsushiro/Japan	1997-07-01~1999-12-31	-3.334	2334.66	4.6403×10^{-2}	-4.85485×10^{-7}
Membach/Belgium	1997-07-01~2000-05-31	-3.428	-909.798	-4.9404×10^{-6}	1.37124×10^{-7}
Metsahovi/Finland	1997-07-01~2000-06-30	-3.810	-1854.78	2.89513×10^{-2}	-2.69912×10^{-7}
Strasbourg/France	1997-07-01~1999-07-31	-3.000	2.56017	1.53173×10^{-3}	3.06189×10^{-8}
Syowa/Antarctic	1997-07-01~1998-12-31	-3.920	-1914.72	-8.6945×10^{-3}	-2.89515×10^{-7}
Vienna/Austria	1997-07-01~1999-06-30	-3.220	-4995.73	4.39883×10^{-3}	-1.24985×10^{-7}
Wetzell/Germany	1996-07-28~1998-09-23	-3.484	2353.82	-2.8184×10^{-1}	-3.79209×10^{-7}
Wuhan/China	1997-12-20~2000-08-31	-3.498	3111.63	4.89498×10^{-3}	-1.43076×10^{-7}

3 Estimation of the Power and Product Spectral Density

Based on the Fourier transform technique, we estimate the spectrum for a given tidal gravity time series follows the methods of *Smylie,* [1993a]. However a suitable averaging method should be selected in order to increase reliability of the results. In our case, the observations with total length T

are split into several segments, each of which has a common length M with 75% overlap. Hence the number of the data segments κ is given as

$$\kappa = 4 \cdot T/M - 3 . \tag{2}$$

The Fourier transform of the n^{th} segment may be written as

$$F(n;\omega) = \int_{-\infty}^{+\infty} Res(t) \cdot w(t) \cdot e^{-i\omega t} dt , \tag{3}$$

where ω denotes the angular frequency and $w(t)$ is a chosen window function with a common length M and i the imaginary number. The Fourier transform of the full residual series can be evaluated by averaging over the results of all the κ segments, expressed as

$$F(\omega) = \frac{1}{\kappa} \sum_{n=1}^{\kappa} F(n;\omega) = \tilde{A}(\omega) \cdot e^{i\tilde{\varphi}(\omega)} , \tag{4}$$

where $\tilde{A}(\omega)$ and $\tilde{\varphi}(\omega)$ are the amplitude and phase. Therefore the estimation of the power spectral density can then be conveniently deduced as

$$\tilde{P}(\omega) = F^*(\omega) \cdot F(\omega)/I = \tilde{A}^2(\omega)/I , \tag{5}$$

where I is the normalisation factor given as

$$I = \int_{-M/2}^{M/2} w^2(t) dt \tag{6}$$

When using N different time series, if the Fourier transform of one series is denoted as $F_i(\omega) = \tilde{A}_i(\omega) \cdot e^{i\tilde{\varphi}_i(\omega)}$, and its power spectral density expressed as $\tilde{P}_i(\omega)$ (with i=1, 2, ..., N), then the product spectral density (PSD) estimate $\overline{P}(\omega)$ can be defined as

$$\overline{P}(\omega) = \left[\prod_{i=1}^{N} \tilde{P}_i(\omega) \right]^{\frac{1}{N}} = \left\{ \prod_{i=1}^{N} \left[F_i^*(\omega) \cdot F_i(\omega)/I \right] \right\}^{\frac{1}{N}} = \left[\prod_{i=1}^{N} \tilde{A}_i^2(\omega)/I \right]^{\frac{1}{N}} \tag{7}$$

This expression is equivalent to the cross spectral density estimation given by *Hinderer et al.* [1995]. Based on equation (5), the individual power spectral densities for all 21 residual series are obtained. The selected length for common segment is taken as M=12000h and the Parzen window is chosen as the time domain window. The Product Special Density (PSD) signals for both G-I and G-II, stacked based on equation (7), are then computed. As a convenient comparison, the PSD estimations for station barometric pressure are also computed.

It is seen that the plots of the PSD estimate for barometric pressure for G-I and G-II are very similar, showing similar properties of the station pressure. Two significant spectral peaks relating to solar heat tides (S5 and S6) in sub-tidal band are noted. The analysis shows that although the atmospheric pressure signals are removed from original tidal gravity records with a single coefficient, however, it is not sufficient to remove them entirely due to the frequency dependence of the admittance [*Merriam*, 1993; Crossley 1995, *Sun,* 1995; *Sun,* 1997; *Kroner and Jentzsch* 1999]. Moreover S5 and S6 waves are coherent harmonic signals at planetary scale that is not true for the background noise. This is the reason why the corresponding influences of the S5 and S6 signals also appear in the gravity product spectrum. In order to detect effectively the weak geodynamical signals, it is necessary for us to remove further the remaining pressure signals. Using a cubic polynomial, the mean station background noises are simulated in sub-tidal band.

The ratios of gravity and of pressure product spectral amplitude are taken as the frequency dependent pressure-gravity coefficients for remaining correction for S5 and S6 wave. The linear function between pressure and gravity product spectral amplitude is adopted to fit the coefficients in order to remove further the remaining barometric influence for other wave band. After such correction, the final PSD estimates for both G-I and G-II are shown in Figure 1.

Comparing upper and lower curves in Figure 1, it can be seen that the mean background noise is much lower in G-II than that in G-I. It confirms the high quality SG observations during the GGP period. From Figure 1, there are no obvious peaks relating to the Slichter triplet claimed by *Smylie* [1992b], *Smylie et al.* [1993a, 1993b] and *Courtier et al.* [2000]. However several significant spectral peaks denoted as SP1, SP2, ..., and SP8 are found for both G-I and G-II. What are the sources of these common spectral peaks? In order to find answer, the PSD estimates for both pressure and tidal gravity residuals in G-II at stations inside and outside Europe are also carried out, it is optimal that the similar peaks are situated. This implies that 8 common peaks do not arise from the pressure influence, local background noise and systematic observation errors, it is possible the expression of some hidden common harmonic signals. Besides the 8 common spectral peaks, there exist also two obvious peaks near the SP1 in G-II.

In order to check the effectiveness of a stacking technique in above study, a verification test has been performed. Signal of amplitudes (0.5, 0.7 and 0.9 nGal), at a known frequency, are injected into each gravity residuals series in G-II, then the PSDs for each series are stacked. The selected frequency is located in the central part of our 8 common peaks, i.e., 0.23 cpd. The results show that no common peak appears when injecting a signal with an amplitude 0.5 nGal. However, when injecting a signal with an amplitude 0.7 nGal, the signal to noise ratio is about 1.15 and the peak is marginally identifiable. When using a signal with an amplitude 0.9 nGal, the signal to noise ratio reaches 1.25 and an clear peak is found. This test shows that the stacking technique can effectively detect a common signal with amplitude of one nGal, distributed globally around the world. Therefore the 8 peaks found in our study are approved.

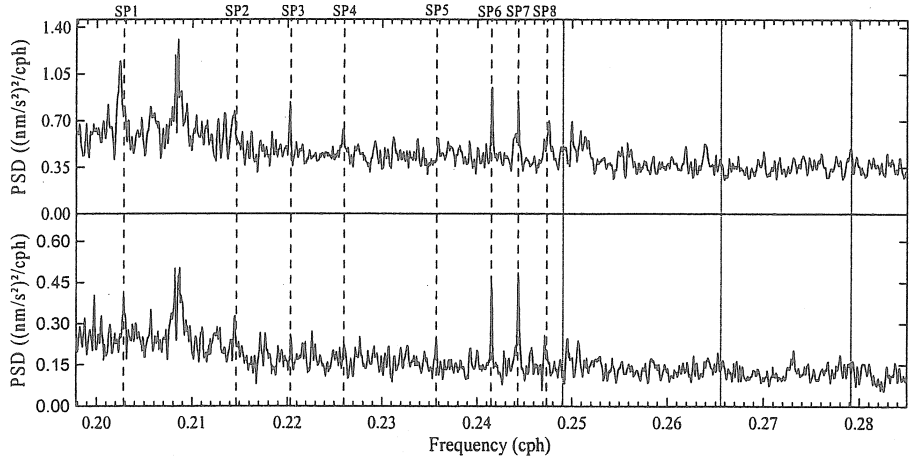

Figure 1. Final product spectral density (PSD) estimates for G-I (upper) and G-II (lower) after further pressure correction. Three vertical solid lines correspond to the locations of the Slichter modes (claimed by *Smylie et al,* 1993, and *Courtier et al.,* 2000). The vertical dashed lines are the locations of the common significant peaks.

4. Identification of the spectral peaks

Now let us determine the resonance parameters, including the central frequencies and periods, quality factors and resonance strengths. As *Smylie* [1992a, 1992b], the eigen-resonance frequency near the spectral peaks are simulated by a harmonic oscillator given as

$$s(f) = \frac{A^2}{1 + 4\left[(f - f_0)/\Delta f\right]^2}, \tag{9}$$

where $s(f)$ is the PSD estimates at frequency f, A resonance strength in $\mathrm{nm \cdot s^{-2} \cdot cph^{-1/2}}$, f_0 central frequency of corresponding spectral peak and Δf damping interval of the resonance frequency. Therefore the central period T and quality factor Q can then be estimated as $T = 1/f_0$ and $Q = f_0/\Delta f$.

The resonance parameters with their error estimation for total of 10 common spectral peaks for both G-I and G-II are determined (Table 2).

From Table 2, one can see that the discrepancy of resonance parameters determined for both groups is very small. Taking an average, the central periods of spectral peak are then obtained numerically. The periods for peaks SP1, SP4 and SP7, as examples, are given as 4.93441 ±0.00186h, 4.42734 ±0.00159h and 4.09380 ±0.00082h. They are surpassingly similar to those of the translational modes, computed theoretically by *Smith* [1976] for model DG579 as 4.916h, 4.441h and 4.055h. The discrepancies are 0.4%, -1.4% and 1.0% respectively. Therefore it is necessary for us to analysis if these common spectral peaks come from the translational oscillation movement of the solid inner core. The SP7 has two large neighbour peaks SP6 and SP8 situated symmetrically which may relate to the eigenfrequeny splitting of the well-known free spheroidal and toroidal oscillation modes due to the Earth's rotation and ellipticity [*Dahle,* 1968, 1969]. A similar splitting appears near SP1 in G-II. These facts could be in favour of the identification of the Slichter triplet with the peaks SP1, SP4 and SP7. However the amplitude of the SP4 is very weak compared with that of SP7 and even of the SP1. It is at the detection limit of gravity signal of 0.7 nGal. Moreover the peak SP7 is located in the frequency band of the six-diurnal tides. In Table 4 we give the main constituents identified for example in the oceanic tides at Oostend in Belgium of *Melchior et al.* [1967]. It is interesting to note that the two main peaks in Figure 7 corresponds to the two largest amplitudes in Table 3 and that peak SP8 is significantly weaker. The wave 2MK6 is probably mixed up with 2SM6 and the wave MSK6 with 2SM6. At the left of the Figure 7 we are in the frequency band of the fifth-diurnal tides, which are not observed in Oostend (Table 4)

Table 2. Resonance parameters of the solid inner core determined when stacking the SG data

	G-I				G-II			
	f_0/cph	T/h	Q	A	f_0/cph	T/h	Q	A
SP1	0.20244	4.93969	94	0.98293	0.20288	4.92907	103	0.56581
	(± 0.00009)	(± 0.00212)	(± 14)	(± 0.02250)	(± 0.00007)	(± 0.00160)	(± 19)	(± 0.01703)
SP2	0.21435	4.66530	121	0.87720	0.21451	4.66185	88	0.51704
	(± 0.00003)	(± 0.00062)	(± 10)	(± 0.00998)	(± 0.00007)	(± 0.00157)	(± 17)	(± 0.01275)
SP3	0.22021	4.54122	96	0.75371	0.22034	4.53841	69	0.43480
	(± 0.00017)	(± 0.00346)	(± 46)	(± 0.03481)	(± 0.00014)	(± 0.00287)	(± 25)	(± 0.01333)
SP4	0.22592	4.42633	100	0.74564	0.22582	4.42835	108	0.44698
	(± 0.00005)	(± 0.00088)	(± 13)	(± 0.01145)	(± 0.00012)	(± 0.00229)	(± 31)	(± 0.01678)
SP5	0.23608	4.23589	66	0.68372	0.23574	4.24199	142	0.42847
	(± 0.00020)	(± 0.00363)	(± 20)	(± 0.01105)	(± 0.00007)	(± 0.00133)	(± 33)	(± 0.01764)
SP6	0.24154	4.14012	184	0.81952	0.24153	4.14036	200	0.52575
	(± 0.00007)	(± 0.00116)	(± 41)	(± 0.04121)	(± 0.00007)	(± 0.00117)	(± 42)	(± 0.03009)
SP7	0.24421	4.09493	162	0.81406	0.24434	4.09269	248	0.59393
	(± 0.00006)	(±0.00092)	(± 29)	(± 0.02427)	(± 0.00004)	(± 0.00072)	(± 35)	(± 0.02634)
SP8	0.24755	4.03952	180	0.78873	0.24722	4.04494	133	0.43971
	(± 0.00004)	(± 0.00064)	(± 32)	(± 0.01862)	(± 0.00007)	(± 0.00119)	(± 25)	(± 0.01624)
S5	0.20833	4.80000	289	1.68925	0.20835	4.79957	335	1.14333
	(± 0.00003)	(± 0.00065)	(± 33)	± 0.06622)	(± 0.00003)	(± 0.00057)	(± 39)	(± 0.04596)
S6	0.24998	4.00027	145	0.93283	0.24987	4.00214	205	0.62452
	(±0.00006)	(± 0.00090)	(± 20)	(± 0.03001)	(± 0.00004)	(± 0.00069)	(± 26)	(± 0.02216)

The wave M5 may explain the very large peak in G-I. The waves 2MO5 and 2SO5 correspond to the small peaks symmetrical with respect to the wave SP1 in G-II. The wave 2SK5 is mixed up with wave S5. The peaks SP2 to SP5, situated between the five- and six-diurnal bands, are not so easily explained but they are generally weaker and close to the detection level illustrated in Figure 8. In the oceanic tides the sixth diurnal tides are called "shallow water components" and are due to non-linear interactions among the main tidal constituents close to the coasts. These generated modes explain why the fifth-diurnal tides are not observed in Oostend as the diurnal tides are very weak in this area.

Fifth-diurnal tides can be produced indeed in places, like China sea, where both diurnal and semi-diurnal oceanic tides are present. As many GGP stations used in this study are close to the sea we could imagine an oceanic tidal loading due to the shallow water components. However these components are restricted to the coastal areas and their loading efficiency is thus very weak. A more evident way of generating fifth- and sixth-diurnal components is the existence of non-linearities in the instruments and their electronics. For example wave M5, which is a clear non-linear term, is large in G-I where we have a majority of old superconducting instruments of lower quality.

Table 3: Six-diurnal tides identified observed in oceanic tides at Oostend harbour and identified in the PSD estimates [Melchior et al., 1967].

Wave	Cycle/hour	Period (h)	Ampl.(cm)	identification
2MN6	0.240022	4.1663	3.7	
M6	0.241534	4.1402	6.8	SP6
MSN6	0.242844	4.1179	1.8	
2MS6	0.244356	4.0924	7.0	SP7
2MK6	0.244584	4.0886	1.9	
2SM6	0.247178	4.0457	1.3	SP8
MSk6	0.247406	4.0419	1.0	

Table 4: five-diurnal tidal frequencies observed in PSD estimates

Wave	Cycle/hour	Period	identification
2MO5	0.199753	5.0062	G-II
M5	0.020128	4.9683	G-I
2MK5	0.202803	4.9309	SP1
2SO5	0.205397	4.8686	G-II
2SK5	0.208447	4.7974	

5 Conclusions and Discussion

The PSD estimates for both G-I and G-II of the SG tidal gravity residuals at 14 GGP stations distributed globally are estimated accurately by using the FFT and a stacking technique in order to confirm the triplet translational resonance of the Earth's solid inner core. The final results indicate that there are no obvious signals in our PSD estimates related to Slichter modes at the frequencies claimed by *Smylie et al.* [1993a, 1993b] and *Courtier et al.* [2000].

Instead, it is found that there exist several common significant spectral peaks in the sub-tidal band, which are not present in barometric pressure series. Unhappily the main peaks are located in the fifth- or sixth-diurnal bands and coincide with the expected frequencies of the non-linear tides. It is probably a pure coincidence if the central periods of three peaks are estimated accurately at 4.93438, 4.42734 and 4.09269, periods in agreement with the eigenperiods of the Slichter modes computed theoretically by *Smith* [1976]. We can conclude that even if the values computed by Smith are correct we shall not be able to confirm them as the spectral peaks will be obscured by the non-linear tides generated either by oceanic effects or instrumental non-linearities.

We can also wonder why the peaks detected by *Smylie et al.* [1993] and *Courtier et al.* [2000] are not visible in our study. Perhaps the Slichter modes are not always exited and we should then apply techniques derived from the wavelet analysis. Another possibility is also that increasing the extension of the network, without taking into account the geographical phase distribution of the Slichter modes, is degrading the coherence of the signal.

Of course, to detect experimentally the dynamic effects of the solid inner core motion and other general core modes is a very complicated task so far. The detecting limit of surface gravity variations is at the level of 0.7 nGal or more when high-precision SG gravimeter observations

recorded at globally distributed stations are used simultaneously. This is nearly the upper limit on the signals induced at the Earth's surface by the geodynamics of the Earth's interior. On the other hand, there is not any convincing theoretical model of the core modes for a realistic Earth so far. Therefore the further investigation depends on the establishment of a reasonable and acceptable theoretical model, to provide the spectral properties of the core modes, and on the further accumulation of the global SG gravity data via the GGP network since they can provide us with more accurate spectral resolution. With that respect it is encouraging to see the improvement in signal to noise ratio in the G-I and G-II.

Acknowledgements

The authors are grateful to David Crossley, the GGP Chairman from St. Luis University, USA and all the station managers for collecting high quality SG data. Marque Hendrickx and Leslie Vandercoilden from Royal Observatory of Belgium take part in data pre-process. HP Sun wishes to thank Doug Smylie for supporting his visit in York University Canada, and for providing with part of codes for computing the power spectral density. HP Sun and JQ Xu acknowledge P Paquet for supporting to visit Royal Observatory of Belgium and the International Centre for Earth Tides. This research is also partly supported by the key project of the knowledge innovation of Chinese Academy of Sciences (No.KZCX3-SW-131), Natural Sciences Foundation of China (No.40374029), China-Belgium scientific cooperation project via the Ministry of Sciences and Technology of China (No.2002CB713904) and the Belgian Office for Federal Scientific, Technical and Cultural Affairs.

Reference

[1] Aldridge, K., and L. I. Lumb, Inertial waves identified in the Earth's fluid outer core, *Nature, 325,* 421–423, 1987.

[2] Courtier, N., B. Ducarme, J. Goodkind, J. Hinderer, Y. Imanishi, N. Seama, H. P. Sun, J. Merriam, B. Bengert, and D. E. Smylie, Global Superconducting gravimeter observations and the search for the translational modes of the inner core, *Phys. Earth Planet. Inter., 117,* 3–20, 2000.

[3] Crossley, D. J., Jensen O. G., Hinderer J. Effective barometric admittance and gravity residuals. *Phys. Earth Planet. Int.,* 90, 221-241, 1995.

[4] Crossley, D., J. Hinderer, G. Casula, O. Francis, H. T. Hsu, and et. al., Network of superconducting gravimeters benefits a number of disciplines, *Eos, Transactions, American Geophysical Union, 80*(11), 121, 125–126, 1999.

[5] Cummins, P., J. Wahr, D. Agnew, Constraining core undertones using stacked IDA gravity records, *Geophys. J. Int., 106,* 189–198, 1991.

[6] Dahlen, F. A., The normal modes of a rotating, elliptical Earth. *Geophys. J. Roy. Astron. Soc., 16,* 329–367, 1968.

[7] Dahlen, F. A., The normal modes of a rotating, elliptical Earth-II Near-resonance multiplet coupling, *Geophys. J. Roy. Astron. Soc., 18,* 397–436, 1969.

[8] Ducarme B., H. P. Sun, and J. Q. Xu, New Investigation of Tidal Gravity Results from the GGP Network, *Bull. Inf. Marées Terr., 136,* 10761–10775, 2002.

[9] Ducarme, B., and H. P. Sun, Tidal gravity results from GGP network in connection with tidal loading and earth response, *J. Geodetic Society Japan, 47*(1), 308–315, 2001.

[10] Goodkind, J. M., The SGs principles of operation, current performance and future prospects. In: Poitevin C. (Ed.), *Proc. workshop non-tidal gravity changes*, Luxembourg, 81–90, 1991.

[11] Hinderer, J., D. Crossley, and O. Jensen, A search for the Slichter triplet in superconducting gravimeter data, *Phys. Earth Planet. Inter., 90,* 183–195, 1995.

[12] Jensen, O, J. Hinderer, and D. Crossley, Noise limitations in the core-mode band of superconducting gravimeter data, *Phys. Earth Planet. Inter., 90,* 169–181, 1995.

[13] Kroner, C., and G. Jentzsch, Comparison of different barometric pressure reductions for gravity data and resulting consequences, *Phys. Earth Planet. Inter., 115*, 205–2187, 1999.

[14] Melchior, P., and B. Ducarme, Detection of inertia gravity oscillations in the Earth's core with a superconducting gravimeter at Brussels, *Phys. Earth Planet. Inter., 42,* 129–134, 1986.

[15] Melchior, P., P. Pâquet, and C. Van Cauwenberghe, Analyse harmonique de vingt années d'enregistrements de marées océaniques à Ostende, *Observatoire Royal de Belgique, Communications, Série B, 20,* 1967.

[16] Merriam, J. B., The atmospheric pressure correction in gravity at Cantley, Quebec, *In: H.T. Hsu ed. Proc. 12th Int. Sympos. Earth Tides, Beijing, Science Press,* 161–186, 1993.

[17] Richter, B., Parallel registration with two superconducting gravimeters, *Bull. Inf. Marées Terr., 99,* 6757–6758, 1987.

[18] Slichter, L .B, The fundamental free mode of the Earth's inner core, *Proc. Natl. Acad. Sci., USA, 47*, 186–190, 1961.

[19] Smith, M. L., The scalar equations of infinitesimal elastic-gravitational motion for a rotating, slightly elliptical Earth, *Geophys. J. R. astr. Soc., 37,* 491–526, 1974.

[20] Smith, M. L., Translational inner core oscillations of for a rotating, slightly elliptical Earth, *J. Geophys. Res., 81*(17), 3055–3064, 1976.

[21] Smylie, D. E., and D. G. McMillan, The inner core as a dynamic viscometer, *Phys. Earth Planet. Inter., 117,* 71–79, 2000.

[22] Smylie, D. E., and M. G. Rochester, Compressibility, core dynamics and the subseimic wave equation, *Phys. Earth Planet. Inter., 24,* 308–319, 1981.

[23] Smylie, D. E., and X. H. Jiang, and B. J. Brennan, Numerical calculation of modes of oscillation of the Earth's core, *Geophys. J. Int., 108,* 465–490,1992b.

[24] Smylie, D. E., J. Hinderer, and B. Richter, The product spectra of gravity and barometric pressure in Europe, *Phys. Earth Planet. Inter., 80,* 135–157, 1993a.

[25] Smylie, D. E., The inner core translational triplet and the density near the Earth's centre, *Science, 255,* 1678–1682, 1992a.

[26] Smylie, D. E., Viscosity near Earth's solid inner core, *Science, 284,* 461–463, 1999.

[27] Smylie, D. E., X. H. Jiang, Core oscillations and their detection in superconducting gravimeter records, *J. Geomag. Geoeletr., 45,* 1347–1369, 1993b.

[28] Sun, H. P., Atmospheric gravity Green's function, *Chinese Science Bulletin*, 1997, 42(20): 1712–1719.

[29] Sun, H. P., B. Ducarme, and X. J. Xu, Preliminary results of the free core nutation eigenperiod obtained by stacking SGobservations at GGP stations, *Bull. Inf. Marées Terr., 136,* 10725–10728, 2002a.

[30] Sun, H. P., H. T. Hsu, J. Q. Xu, X. D. Chen, and X. H. Hao, Determination of the new tidal parameters obtained with a superconduction gravimeter at station Wuhan/China, *J. Geodetic Society Japan, 2001, 47*(1): 347–352, 2001b.

[31] Sun, H. P., H.T. Hsu, and Y. Wang, On the calibration of a superconducting gravimeter GWR–C032 with an absolute gravimeter FG-5 in Wuhan, *Bull. Inf. Marées Terr., 135,* 10639–10642, 2002c.

[32] Sun, H. P., H.T. Hsu, G. Jentzsch, and J. Q. Xu, Tidal gravity observations obtained with superconducting gravimeter and its application to geodynamics at Wuhan/China, *J. Geodynamics, 33*(1-2): 187–198, 2002b.

[33] Sun, H. P., J. Q. Xu, and B. Ducarme, Experimental Earth tidal models of the core resonance obtained by stacking tidal gravity observations from GGP Stations, *Bull. Inf. Marées Terr., 136,* 10729–10733, 2002d.

[34] Sun, H. P., Static deformation and gravity changes at the Earth's surface due to the atmospheric pressure, [Ph. D. thesis], *Serie Geophysique No. Hors-Serie, Royal Observatory of Belgium, Brussels,* pp280, 1995.

[35] Sun,H. P., S. Takemoto, H.T. Hsu, T. Higashi, and A. Mukai, Precise tidal gravity recorded with superconducting gravimeters at stations Wuhan/China and Kyoto/Japan, *J. Geodesy, 74,* 720–729, 2001a.

[36] Tamura, Y., A harmonic development of the tide-generating potential, *Bull. Inf. Marées Terr., 99,* 6813–6855, 1987.

[37] Vauterin, P., Tsoft: Graphical and interactive software for the analysis of Earth tide data, *In: Ducarme B and Paquet P ed., Proc. 13th Int. Sympos. Earth Tides, Brussels,* 481–486, 1998.

[38] Warburton, R., GWR superconducting gravimeter operation manual, *GWR instruments company*, San Diago, USA, 1985.

[39] Wenzel, H. G., Earth tide data processing package ETERNA 3.30: the nanoGal software, *In: Ducarme B and Paquet P ed., Proc. 13th Int. Sympos. Earth Tides, Brussels,* 487–494, 1998.

[40] Xu, J. Q., H. P. Sun, and S. C. Luo, Study of the Earth's free core nutation by tidal gravity data recorded with international superconducting gravimeters, *Science in China (Series D), 45*(4), 337–37, 2002a.

[41] Xu, J. Q., Study and detection of the geodynamics effects of the fluid outer core of the Earth, [PhD thesis], *Institute of Geodesy and Geophysics, Chinese Academy of Sciences,* pp125, 2002b.

AN ATTEMPT TO OBSERVE THE EARTH LIQUID CORE RESONANCE WITH EXTENSOMETERS AT PROTVINO OBSERVATORY

E.A.Boyarsky[1)], B.Ducarme[2)3)], L.A.Latynina[1)], L.Vandercoilden[3)]

[1)]*Gamburtzev Institute for Physics of the Earth, RAS, Moscow*

[2)]Chercheur Qualifié FNRS, [3)]*Royal Observatory of Belgium, Brussels*

ABSTRACT

We performed a tidal analysis of the strain records obtained at the Protvino observatory near Moscow during the years 1995–2000. The deformations were measured with four 16 m long extensometers installed in the NS and EW directions at a depth of 15 m. This study is focusing on the liquid core resonance effect. We are using the ratios of the amplitude factors of the resonant waves K1 and P1, to the amplitude factor of the static wave O1. The ratios are in principle free from indirect effects, such as cavity effects, which are roughly similar for all the diurnal waves. The resonance effect is clearly recognized in the measured ratios, especially in EW direction. The main cause of discrepancy between the observed and theoretical values of the resonance is the diurnal outer temperature variation, while the influence of the inner temperature and of the atmospheric pressure is many times lower. The temperature response was first directly evaluated as additional unknown in the tidal analysis and was also computed for various time shifts τ of the temperature signal. As the improvement was not so effective for the NS component a special study was performed. An attempt was made to determine the temperature response from the S1 wave alone or to include also the time derivative of the temperature. All attempts gave similar results: the temperature compensation increases the amplitude of K1 and decreases the amplitude of P1, while O_1 is practically not affected. K1 becomes closer to the expected resonant value. It is not quite clear, to what extend the correction, simply based on the outer temperature variations, is physically valid, as the perturbations are due to the thermoelastic strains. In their turn, the latter can be governed by the spatial distribution of the surface temperature and the mechanical properties of the rocks, including not only their values but also their spatial and temporal gradients.

1. Introduction

The tidal deformations depend on the regional and local features of the Earth crust and mantle. Tidal deformation monitoring is useful for the studies of the structure and evolution of crustal blocks, in zones of active tectonic processes of natural and industrial origin [Starkov et al. 1992]. Data collected by the tidal gravity networks are contributing to the determination of the regional irregularities of the Earth crust and upper mantle [Yanshin et al. 1986].

Extensometer data can be used in global problems such as the investigation of the nearly diurnal resonance of the Earth liquid core. This resonance, on a frequency 1.004915 cycle per solar day, disturbs the amplitudes of tidal diurnal waves with close frequencies i.e. P_1 and K_1. The tides and the forced nutations are produced by common gravitational forces but expressed in alternative coordinate systems: the nutations—in the inertial one, the tidal oscillations —in the terrestrial one. The corresponding frequencies differ only by the sidereal frequency 1.0027379 cycle per solar day. The Tidal wave K_1 corresponds to the precession, while the tidal wave P_1 corresponds to the half-yearly nutation. The forced nutations are globally observed using the techniques of astronomy and space geodesy. The tides are studied locally by geophysical methods. Until recently the earth tidal observations played a prevailing role in investigation of the Earth core

resonance effects. In the last decades the vigorous progress of the space geodesy inversed the roles. Nevertheless, precise tidal gravity observations by means of superconducting gravimeters open new perspectives in the investigation of the liquid core resonance effects as they register reliably the tidal waves P_1, K_1, PHI_1 and PSI_1 which are the closest to resonance and hence highly influenced (Ducarme & al., 2002). The extensometers have an essentially lower precision. But they hold much promise if one considers that changes of the Love numbers at frequencies near to resonance induce relative disturbances in strain that are ten times larger than in gravity tide (Fig.1).

The theory of the luni-solar nutations and tides, taking into account nearly diurnal resonance of the liquid core, was developed by M.S.Molodensky [1961] and became the basis for numerous works later. The most thorough computations of the body tide for rotating earth, having elliptic stratification, self-gravitation and a solid inner core, were performed by J.Wahr [1981] for different models of the Earth. New approaches to the data analysis for the forced and free nutations of the Earth allowed to E.Groten and S.M.Molodensky [1996] and S.M.Molodensky [1999] to create an optimal model of the tides. Using modern VLBI-observations, they determined with a significant accuracy the Q-factors of the bottom mantle and the dynamical flattening of the liquid core. Dehant & al. [1999] proposed tidal models including non hydrostatic flattening of the Earth and inelasticity in the mantle. Mathews & al. [2002] introduced a magnetic coupling between core and mantle.

Let us consider the theoretical amplitude of the diurnal tidal deformations in two orthogonal directions [Melchior 1972]:

for NS: $A_{\theta\theta} = W_2 / ag \times (h - 4l) = A \times (h\text{-}4l)$,

for EW: $A_{\lambda\lambda} = W_2 / ag \times (h - 2l) = A \times (h\text{-}2l)$.

Here W_2 is the tidal potential of degree two, a is the equatorial radius of the Earth, g is gravity at its surface, h and l are the Love's and Shida's numbers for a given tidal frequency. An effect of the liquid core resonance appears as changes in the numbers h and l and can be determined from the amplitude factor $\varphi_{xx} = A_{xx}/A$ of a resonant tidal wave. The amplitude factor of a single wave is not adequate for determination of resonance effect as far as an observed amplitude contains always "indirect" effects associated with topography, irregularities of geology etc. But these indirect effect are almost the same for all the diurnal tidal waves and can be eliminated by considering the ratio of the amplitude factor of a resonance-disturbed wave to that of an undisturbed wave [Latynina 1983].

We shall thus estimate how the resonance affects the waves P_1 and K_1 by taking ratios of their amplitude factors φ_{xx} to that of O_1. The amplitudes of these three waves are rather large and measured reasonably well. The wave O1, which is far from resonance, is chosen as reference. The resonance changes the amplitude of a wave close to it, so the ratio of its amplitude factor to that of O_1 becomes different from one. Theoretically estimated ratios vary in a small range of 1 to 2 percent according to the different Earth models. The averages for NS and EW components for different models are:

$\varepsilon_{P1} = \varphi_{NS}(P_1) / \varphi_{NS}(O_1) = 0.90$ $\qquad$ $\varepsilon_{K1} = \varphi_{NS}(K_1) / \varphi_{NS}(O_1) = 0.65$

$\eta_{P1} = \varphi_{EW}(P_1) / \varphi_{EW}(O_1) = 0.94$ $\qquad$ $\eta_{K1} = \varphi_{EW}(K_1) / \varphi_{EW}(O_1) = 0.80.$

In opposition to Polzer at al. [1996] we consider here the ratio of the amplitude factors but not their difference.

2. Data analysis

We are studying here the extensometer measurements made at Protvino observatory (54°52′ N, 37°13′ E) located 100 km southward from Moscow. The quartz 16-m extensometers are placed at a depth of 15 m in horizontal galleries along NS and EW directions (Fig.2) [Latynina et al. 1997, Boyarsky et al. 2001]. The enclosing rocks consist of sandstone and marl layers and jointed limestone. During the years seventies and eighties analog recording was used, and time registration was not accurate. As a result, only some short observation series could be taken for the tidal analysis [Karmaleeva 1999]. In this work we use only the observations of 1995–2000. However the most reliable data are available since digital acquisition systems were installed, with 12-bit ADC in 1998 and 16-bit ADC in 1999.

The harmonic analysis of the measurements is performed with Eterna 3.0 program [Wenzel 1996], using the Pertsev filter with a length of 51 hours. The measurement intervals in Table 1 overlap slightly. Otherwise they would be too short for the separation of the waves P_1, S_1, and K_1, which requires one year time interval. Detailed analysis results (Tables 2 to 5) are given only for the most reliable part (1999–2000). The results of the three EW strainmeter signals are rather coherent. The discrepancy is of the order of 5% on the main wave O_1 (Table 6).

For the NS component the value of ε_{K1}, reflecting FCN resonance effects, significantly differs from the theoretical model (Table 1). The difference is still large if one takes only the more reliable recent measurements. The average EW ratio η_{K1} from three intervals is not so far from the rated one. But for the wave P_1, which has less resonance effect, the observed ratio η_{P1} contradicts physical notions. For the years 1999–2000 the discrepancies between observed and theoretical values of η are larger than 10%. However the comparison of the three EW extensometric signals for the same time interval 1999–2000 (Table 1) confirms that the η values are in good internal agreement: 2% for P_1 and 6% on K_1. The use of the amplitude ratios did not suppress the systematic errors. According to hydrological measurements in the borehole, diurnal level variations of the upper aquifer at a depth of 25 m are less than 1 cm. There are no more accurate and complete related data, so this point needs further studies. To our opinion, the remaining discrepancy with the theoretical value is mainly associated with the meteorological noise.

3. Influence of temperature variations on tidal amplitudes

The measurements are affected by meteorological influences. That can be seen directly from the extremely large values of wave S_1 in Tables 2 to 5. Its amplitude factor in the reliable data of 1999–2000 was 67.3 for NS direction and 30.2–32.9 for the strainmeters in EW direction. The simplest way to compensate meteorological influences is to evaluate the responses (regression coefficients) R to selected meteorological parameters. We have thus to find the perturbation mechanism. The direct exposure of the deformation sensors to temperature variations is small. The seasonal temperature wave inside the galleries reaches only 0.3°, and the diurnal variations do not exceed 0.01°, as long as nobody is entering

the station. Induced errors on the capacity sensors are an order of magnitude lower than the observed diurnal deformations, and thermo-expansion of the extensometer quartz tube is tens times less than that of enclosing rock. It is of much importance, that the spectrum of temperature inside the stations contains only noise near the frequency 1 cycle per day (Fig. 3, below). On the contrary, the spectrum of the outer temperature (Fig.4) contains, as it should be, a sharp peak at the frequency one cycle per day with side lobes at the P_1 and K_1 frequencies which represent the annual modulation of S_1. The whole resonance spectrum will thus be disturbed. It appears, that the most probable sources of transfer of the heat disturbances are thermoelastic deformations of rocks, induced by the outer temperature variations, that propagate tens of meters down.

Consequently, we introduced in the harmonic analysis of the 1999–2000 data sets linear regression coefficients of the observed deformations with respect to the air temperature registered at Serpukhov weather station, 15 km apart as well as to the atmospheric pressure at Protvino observatory (Table 7). The discrepancies between the model values of ε and η and the observed values are largely reduced for K1, especially in EW direction, but P1 is not improved. The atmospheric pressure influence is one order of magnitude lower than the temperature effect. An account of the response to the pressure decreases A_{S1} and residuals but only by few percents (Table 7). A time shift of pressure values in any direction does not affect results.

Therefore the main attention was paid to the temperature effects. The temperature influence was studied at various time shifts τ of the temperature relative to observed deformations, namely $-50^h < \tau < 50^h$ (Fig. 5–6). With this convention a positive time shift of the perturbing signal corresponds to a "time lag" of the strainmeter response. The graphs for the two other EW extensometers are omitted, because they are practically identical to Fig.6. It is supported once more, that the wave O1 is free from diurnal temperature variations. Criteria for the best compensation of temperature effect can be: minimum amplitude A_{S1} of the wave S1, minimum standard deviation s_0 of residuals, maximum absolute value of response R. It is pertinent to note that a behavior of $R(\tau)$ is equivalent to a cross-covariance function.

Diurnal oscillations of R and double-frequency oscillations of A_{S1} and s_0 are explained with repetitive temperatures on adjacent days. These oscillations, naturally, decay with moving from $\tau = 0$ in both direction. In general, a time lag of thermoelastic deformations with respect to temperature variations is quite possible, especially at a depth of 15 m, but not with a lag of 12 or 24 hours, which are only mathematical artefacts. Regional thermoelastic deformations of hundreds kilometers in dimension can be associated only with very small τ of less than one hour. A similar influence of atmospheric pressure variations for tiltmeter measurements has been already reported [Boyarsky et al. 2001]. But any negative τ can meet objections because it is hard to model a physical mechanism that manifests itself in deformations preceding the temperature variations, except if we consider that the effect depends also of the gradients of the harmonic exciting functions.

For the three EW instruments a minimum A_{S1} and the best coincidence of the observed resonance effect with the theoretical one for K1 occur at time shifts of

–0.5, –0.4, and –0.6^h. However, minimum s_0 and maximum R occur uniformly at shifts of +2.3, +2.2, and +2.1^h, with values η_{K1} close to 0.75.

With temperature correction, the amplitude A_{S1} for NS component decreases 4–5 times. Minimum A_{S1} corresponds to a shift $\tau = -0.8^h$ (Table 9), and simultaneously the deviation of the ratio $\varepsilon_{K1} = 0.55$ from its theoretical value 0.65 is minimum (14%) almost at the same τ. Maximum R (0.956 nstr per degree) is at $\tau = +0.6^h$, and the same shift is just a minimum for s_0. Minimum ε_{P1} is rather near ($\tau = +0.9^h$), but corresponds to a maximum of discrepancy with the model. Another criterion to check if the temperature correction is optimal can be the wave K1 phase shift κ_{K1} (Table 9) that should become minimum. Its minimum 1.9 degrees is at $\tau = +2.0^h$.

As already pointed out, a positive time shift τ is preferable from a physical viewpoint as it corresponds to a time lag of the elastic response of the rock. Moreover the oscillations of both s_0 and R decay faster than A_{S1} with larger time shifts. Therefore, the criterion of minimum s_0 and maximum R is better, at least in our case, than the criterion of minimum A_{S1}. It is confirmed by an additional test. We introduced the temperature signal together with its time derivative to derive the optimum phase lag of the strain coupling. It is justified by the fact that the temperature signal is largely dominated by S1 and can be written in first approximation as

$$T = A \cos\omega_1 t \tag{1}$$

and the strain response as

$$RA \cos(\omega_1 t - \kappa) = R_C A \cos\omega_1 t + R_S A \sin\omega_1 t \tag{2}$$

where R is the response and κ the phase lag of the system.

Using the temperature and its time derivative we get

$$R^*_C A \cos\omega_1 t - \omega_1 R^*_S A \sin\omega_1 t \tag{3}$$

and can derive easily (R_C, R_S) from (R^*_C, R^*_S) and thus R and κ.

Experimentally we obtained (Table 9) $R = 0.973$, $\kappa = 8°.5$, $\tau = 0.56^h$, $s_0 = 3.162$. We effectively confirm that a maximum of R and a minimum of s_0 corresponds to a lag of 0.6^h.

The influence of seasonal temperature variations on tilts at Protvino was studied by the authors [Boyarsky and Latynina 1999, Latynina and Boyarsky 2000]. The analysis of short tiltmeter observation series showed that the amplitude of the diurnal waves varies during a year more than twice. Temperature variations affect the measurements with 16 m extensometers to much less extend, especially as they are averaged on rather long series. But the aim of this work—the study of resonance effects—requests very precise tidal parameters.

Temperature disturbance of the gravity tide were studied in details by T.Chojnicki [1987] for Askania GS–11 gravimeters. By means of iterations the temperature wave S1 was eliminated from the observations. The decrease of A_{S1} and s_0, computed from corrected observations, was taken as a criterion. However, the method does not give accurate quantity estimates. Besides, the final result can

depend upon the initial choice of the parameters of the nearly diurnal tidal waves, which have been subtracted from the observed data at the very first stage.

The waves P_1, S_1, K_1 are heavily disturbed by temperature variations. It is easily explained by the characteristics of these variations. The amplitude of diurnal temperature wave S1 is changing along a year. For example, the diurnal variations of the outer temperature at Protvino in summer are about twice larger than in winter. It can be sketchy presented by modulating the amplitude of S_1 by a wave of one year period [see also Merriam 1994]:

$$T(t) = A\ \{1 + B\ (\cos \omega_2\, t)\}\ (\cos\, \omega_1 t), \tag{4}$$

where $\omega_1 = 1/\text{day}$, $\omega_2 = 1/365.25\ \text{day} = 0.00273785$. Hence:

$$T(t) = A\ \cos\, \omega_1 t + AB\{\cos(\omega_1 + \omega_2)\, t + \cos(\omega_1 - \omega_2)\, t\}. \tag{5}$$

Thus, the yearly amplitude modulation of the diurnal temperature wave is equivalent to producing waves with frequencies $(\omega_1 - \omega_2) = 0.99726$ and $(\omega_1 + \omega_2) = 1.00274$, but these are just the frequencies of P1 and K1.

This is clearly seen on the spectrum of the outer temperature (Fig.4), in which we can see not only a sharp diurnal peak with amplitude of 2.3 degrees but also waves with frequencies of 1.0027 and 0.9973 and an amplitude reaching 1.6 degree. Detectable harmonics with frequencies $(\omega_1 + n\omega_2)$, where $n = \pm 2, \pm 3$ etc, indicate a more complicated temperature trend than the simplest model above. Note that at $n = +2$ and $n = +3$ we deal with tidal waves PSI_1 and PHI_1 which are the closest to the resonance.

A direct compensation of the temperature influences with Eterna program (Table 7), even with the application of various time shifts (Fig. 5–6 Table 9), decreased the discrepancy between observed and rated resonance effects for K_1 but not for P_1, especially in NS component. This problem led us to compute directly the contribution of thermoelastic deformations to amplitudes of P_1 and K_1. As well as in Eterna program, it was assumed, that the thermoelastic part of each diurnal wave is proportional to the corresponding temperature variation, namely

$$D(t) = RT(t + \tau), \tag{6}$$

where D is the temperature contribution to the observed deformation. The outer temperature was treated by Eterna program with the identical parameters and on the same time intervals as NS deformations of 1999–2000 (see Table 8, row 3). We assume the adjacent waves have similar response R and phase shift κ. The observed deformation wave S1 is almost entirely of weather origin, mostly of temperature. It makes possible to find the common characteristics R and κ from S1 and calculate thermoelastic contributions to waves P_1 and K_1 which should be subtracted from measured deformations. We find for the thermal S1wave a phase shift of $-7.2°$ with respect to the strain wave, corresponding to a time shift of 0.48^h. Here also P_1 amplitude decreases after correction while K_1 increases. It should be noted that the phase difference becomes closer to zero (Fig.7) in better agreement with the theoretical tidal waves.

The calculated response of –0.75 nstr/Kelvin is rather similar to the value obtained by Eterna program for the global tidal signal. A negative value of R means that rocks compress at depth when outer temperature increases. An incomplete compensation of weather noise in K_1 and no compensation in P_1 imply, that temperature effects are not correctly taken into account or that some weather factors are ignored. Perhaps, the analysis should be made separately for all the

summer and all the winter observations, but we have not yet enough reliable data for that.

The discrepancy between observed and theoretical resonance effects can be associated with a non-adequate model of development of thermoelastic strains. Eterna program assumes linear regression between the rock deformation and the temperature variations. Nevertheless, thermoelastic deformation can be due as well to surface temperature gradients or irregularities of earth crust surface layers, including topography. Let us write the temperature variations be a function of time and place in a form:

$$T(t,x) = A \sin(\omega_1 t)\,(1 - p \cos(x/L)), \tag{7}$$

where p is a constant, and L is length of temperature wave on earth surface along X axis. Then the temperature gradient along X axis is

$$\text{grad}(T) = (A\,p/L) \sin(x/L) \sin(\omega_i t). \tag{8}$$

If the wavelength L does not vary with time, then the responses of the crust to the temperature and its gradient differ only in a constant factor $C = L \sin(x/L)$. Therefore, the attempted compensation of temperature noise is still valid.

Suppose the wavelength L varies with time. This is rather possible because in winter the snow levels off the contrasts in spatial distribution of surface temperature due to the various albedo's of forest, field or water. In this case L can be represented, for example, as

$$L = 1 / (a_1 + a_2 \cos \omega_2 t), \tag{9}$$

where ω_2 is frequency of the yearly wave, a_1 and a_2 are constants. As a result, the harmonics with frequencies $(\omega_1 - 2\omega_2)$, wave PI_1, and $(\omega_1 + 2\omega_2)$, wave PSI_1, will appear in the temperature spectrum. But we could not detect reliably those harmonics in the strain signal, even if we combine all the data at our disposal.

The surface temperature distribution and the structure of the very upper crust layers have a complicated character. It is possible to create a model of thermoelastic deformations corresponding to the conditions of Protvino observatory. Temperature gradients can be associated with the regional geologic structures. Rather monolith blocks of some kilometers in dimension are separated by ancient fracture zones. Under such situation the wavelength L should be comparable with the block dimensions. A differential warming up of ground under the observatory building and its immediate grass surrounding can be a cause of intensive thermoelastic deformations as well. The extensometers themselves are placed in such a manner, that one end of each is under the observatory building, and the other is 10 m apart from the building. Temperature wavelength can have an order of some tens meters. It is very hard to eliminate errors induced with local irregularities. Nevertheless, these considerations should be kept in mind when choosing a place for future observations.

4. Conclusions

The tidal strain deformations at the Protvino observatory, near Moscow, are studied for the period 1995–2000. The deformations were measured with four 16 m extensometers at depth of 15 m (one along NS direction, and three along EW). The computations were made with Eterna 3.0 on three time intervals, more than 1 year each. The total data set exceeds 1200 days. Differences in amplitudes of the main

waves from the three parallel EW extensometers do not exceed 3%, increasing our confidence in the analysis results.

We studied the liquid core resonance effect through the waves K_1 and P_1, using the ratios of their amplitude factors to the amplitude factor of wave O_1. We proceeded from the assumption, that the ratios are free from indirect effects as they are roughly similar for all the diurnal waves. The wave O_1 was taken as reference because its amplitude is of the same order and almost free from resonance effect. The observed resonance disturbances is close to the rated values in the EW direction but not for NS direction.

The main cause of discrepancy between observed and theoretical values is diurnal outer temperature variations. They are responsible of more than 90% of the anomalous large amplitude of the wave S_1. The atmospheric pressure influence is many times less. The data of an adjacent weather station were taken for the compensation of temperature effects. The temperature was taken as auxiliary parameter in the tidal analysis using Eterna 3.0 software. The compensation was also studied at various time shifts τ of the temperature relating to the observed deformation. The shift τ for minimum amplitude of S_1 does not coincide with the shift that gives maximum response R and minimum standard residual s_0.

For EW component observed resonance effects for both P_1 and K_1 become close to the theoretical ones. For NS component a summary of the results is given in Table 9. All attempted corrections give similar results: ε_{P1} decreases while ε_{K1} increases and becomes closer to the reference model. The amplitude of S_1 is minimum at $\tau = -0.8^h$. At -1^h shift there is a minimum discrepancy between observed (0.55) and theoretical (0.65) resonance effects for ε_{K1}. For P_1 the temperature compensation gave almost no result. However from a physical point of view we should assume that the ground response follows the temperature excitation and thus that the time shift of temperature has to be positive. It is confirmed by the fit of the temperature and its time derivative which gave the best fit (s_0=3.162) and a response of -0.973 nstr/K for a time shift of 0.56h. Unhappily ε_{K1}=0.506 is still far from the model (ε_{K1}=0.65).

For comparison the tidal waves amplitudes were estimated by computing direct corrections from the temperature waves for P_1 and K_1, under assumption that the S_1 wave is purely of meteorological origin. The amplitude and phases of these temperature waves were computed from a three-years series of outer temperature.

All methods gave similar results: rocks compress at a depth when outer temperature increase and the coefficient is close to –0.9 nstr/Kelvin. Temperature compensation increases amplitude of K_1 and decreases amplitude of P_1. K_1 becomes closer to the theoretical resonance.

There are many possible causes for the incomplete compensation of weather influences. Hydrological effects are not yet investigated in details. It is not quite apparent, to what extent the compensation of outer temperature variations is valid at all. Errors in observations are associated with thermoelastic strains that, in their turn, can be governed with spatial distribution of surface temperature and mechanical features of rocks, taking into account their gradients as well. The applied procedure is valid, if the spatial distribution of temperature does not vary with time. In this case the responses of deformation to the temperature and its gradient differ only in a constant factor. When temperature variations have a

seasonal pattern, the temperature spectrum is perturbed by harmonics with frequencies near the tidal waves PI_1 and PSI_1. The spectrum of the thermoelastic deformations becomes different from the temperature spectrum. Investigation at the PSI_1 and PHI_1 frequencies require more data than at our disposal.

References

1. *Boyarsky, E.A. and Latynina, L.A.*, 1998. The analysis of the tidal parameters on short measurement intervals. Bull. Inf. Marées Terrestres, 130, 10050–10057.
2. *Boyarsky E.A., Vasil'ev I.M., and Suvorova I.I.*, 2001. The study of tilts and strains at the Protvino geophysical station. Izvestiya, Physics of the Solid Earth, 37, No 9, 764–770.
3. *Chojnicki, T.*, 1987.Temperature distortion of tidal observations // Publications of the Institute of geophysics, Polish Academy of Sciences, F–14 (200). Warszawa–Lodz, 1987, 127–141.
4. *Dehant, V., Defraigne, P. and Wahr, J.*, 1999. Tides for a convective Earth. J. Geophys. Res., 104, B1, 1035-1058.
5. *Ducarme B., Sun H.-P., Xu J.-Q.*, 2002. New investigation of tidal gravity results from GGP network. Proc. GGP Workshop, Jena, March 11-15,2002. Bull .Inf. Marées Terrestres, 136, 10761-10776
6. *Groten, E., Molodensky, S.M.*, 1966. Anelastic properties of the mantle and Love numbers consistent with modern VLBI-data. J. of Geodesy, 270, 1, 603–621.
7. *Karmaleeva R.M.*, 1999. Time variations in tidal wave amplitudes from strain data obtained at the strainmeter station Protvino. Izvestiya, Physics of the Solid Earth, 35, No 5, 429–433.
8. *Latynina L.A., Boyarsky E.A., Vasil'ev I.M., Sorokin V.L.*, 1997. Tiltmeter measurements at the Protvino station, Moscow region. Izvestiya, Physics of the Solid Earth, 33, No 11, 949–956.
9. .*Latynina L.A. and Boyarsky E.A.*, 2000. Seasonal Earth tide variations as a model of earthquake precursor. Volcanology and Seismology, 21, 587–595.
10. *Mathews, P.M., Herring, T.A., Buffett, B.A.*, 2002. Modeling of nutation-precession: New nutation series for nonrigid Earth and insights into the Earth's interior. Journal of Geophysical Research (under press).
11. *Merriam J.B.*, 1994: The nearly diurnal free wobble resonance in gravity measured at Cantley, Quebec // Geophys. J. Int., 119, 369–380.
12. *Latynina, L.A.*, 1983. Manifestation of the liquid core resonance effects in tide strains. Bull. Inf. Marées Terrestres. 90, 5938–5951.
13. *Melchior, P.*, 1972. Physique et dynamique planetaires, V. 3 (Geodynamique). Observatoire Royal de Belgique.
14. *Molodensky, M.S.*, 1961. The theory of nutation and diurnal Earth tides // Communs. Obs. R. Belg., 288, 25–56.
15. *Molodensky, S.M.*, 1999. Models of tidal deformations of the Earth consistent with data on its forced nutation // Izvestiya, Physics of the Solid Earth, 35, 4, 1999, 255–259.
16. *Polzer, G., Zűrn, W., Wenzel H.-G.*, 1996. NDFW analysis of gravity, strain and tilt data from BFO. Bull. Inf. Marees Terrestres. 125, 9514–9545.
17. *Srarkov V.I., Latyninna L.A., Karmaleeva R.M., Rissaieva S.D., Starkova E.Ya, Mardonov B.*, 1992. Pramètres des déformations de marée à Djerino d'après les résultats de 19 années d'observations. Bull. Inf. Marees Terrestres, 112, 8177–8186.

18. *Wahr, J.M.*, 1981. Body tides on an elliptical, rotating, elastic and oceanless earth. Geophysical Journal of the Royal astronomical Society, 64, 677–703.
19. *Wenzel, H.-G.*, 1996. The nanogal software: Earth tide data processing package ETERNA 3.30. Bull. Inf. Marees Terrestres, 124, 9425–9439.
20. *Yanshin A.L., Melchior, P., Keilis-Borok, V.I., De Brcker, M., Ducarme, B., and Sadovsky A.M.*, 1986. Global distribution of tidal anomalies and an attempt of its geotectonic interpretation. Proc. 10th Int. Symp. On Earth Tides, Madrid. Consejo Sup. Investigaciones Cientificas, Madrid, 731–756.

Table 1.Ratio of amplitude factors of waves P1 and K1 to amplitude factor of wave O1.

Observation interval	Extenso-meter	Total time interval	Number of observation, days	Ratio of amplitude factors		Standard residual, nstr
				$\varphi_{P1} / \varphi_{O1}$	$\varphi_{K1} / \varphi_{O1}$	
NS component						
1995–1997	NS–1	703	456	0.60±0.04	0.62±0.02	5.2
1997–1999	NS–1	808	391	0.77±0.07	0.30±0.01	3.8
1999–2000	NS–1	619	601	1.01±0.03	0.37±0.01	3.4
Average				0.79	0.43	
Rated value				0.90	0.65	
EW component						
1995–1997	EW–3	707	460	0.88±0.04	0.84±0.02	2.6
1997–1999	EW–3	407	481	0.96±0.03	0.85±0.02	3.6
1999–2000	EW–1	619	577	1.11±0.02	0.76±0.01	4.0
	EW–2	619	*578*	*1.09±0.02*	*0.75±0.01*	*4.1*
	EW–3	619	600	1.09±0.02	0.71±0.01	3.9
Average				1.01*	0.80*	
Rated value				0.94	0.80	

* For calculation of the average value extensometers EW–1 and EW–2 were taken with weight 0.5, as they are two sensors at one common tube.

Table 2. Results of harmonic analysis of observation in 1999–2000. Extensometer NS–1.

	Wave group	Amplitude measured, nstr	Ratio signal/noise	Amplitude factor and its r.m.s.e.		Phase lead, deg. and its r.m.s.e.	
1	Q1	00629	14.3	0.7882	0.0551	–25.94	3.15
2	O1	2.920	63.6	0.7006	0.0110	–1.67	0.63
3	M1	0.312	4.3	0.9513	0.2213	18.88	12.67
4	P1	1.378	32.6	0.7104	0.0218	124.65	1.25
5	S1	3.088	51.8	67.3428	1.2988	–65.56	74.40
6	K1	1.522	33.4	0.2597	0.0078	39.56	0.45
7	PSI1	0.907	21.3	19.7902	0.9310	–23.88	53.35
8	PHI1	0.591	13.7	7.0819	0.5170	–26.78	29.61
9	J1	0.208	5.1	0.6336	0.1236	20.49	7.08
10	OO1	0.160	2.7	0.8942	0.3358	–12.57	19.24
11	2N2	0.175	5.6	0.5773	0.1028	8.14	5.89
12	N2	1.287	32.4	0.6787	0.0209	3.01	1.20
13	M2	6.755	166.7	0.6818	0.0041	6.60	0.23
14	L2	0.219	5.7	0.7832	0.1373	–8.32	7.87
15	S2	3.319	79.2	0.7200	0.0091	37.92	0.52
16	K2	0.744	15.3	0.5938	0.0387	–21.38	2.22
17	M3	0.039	1.0	0.9519	0.9101	–106.36	52.15

Table 3. Results of harmonic analysis of observation in 1999–2000. Extensometer EW–1.

	Wave group	Amplitude measured, nstr	Ratio signal/noise	Amplitude factor and its r.m.s.e.		Phase lead, deg. and its r.m.s.e.	
1	Q1	0.832	15.7	0.6565	0.0417	–5.69	2.39
2	O1	4.874	90.9	0.7366	0.0081	2.86	0.46
3	M1	0.809	11.4	1.5544	0.1368	–27.85	7.84
4	P1	2.514	51.0	0.8164	0.0160	65.62	0.92
5	S1	2.202	31.7	30.2460	0.9538	–75.40	54.66
6	K1	5.192	97.4	0.5579	0.0057	28.89	0.33
7	PSI1	0.549	11.0	7.5463	0.6838	0.83	39.16
8	PHI1	0.834	16.6	6.2927	0.3795	–39.34	21.74
9	J1	0.538	10.7	1.0348	0.0970	–9.49	5.56
10	OO1	0.394	5.8	1.3853	0.2395	–33.22	13.72
11	2N2	0.064	1.4	4.074	3.0007	–132.62	171.93
12	N2	0.256	4.2	2.6189	0.6203	108.17	35.53
13	M2	0.547	11.5	1.0694	0.0930	5.26	5.32
14	L2	0.110	3.7	4.3821	1.1982	93.79	68.64
15	S2	1.630	33.1	6.8520	0.2070	–99.80	11.85
16	K2	0.266	4.8	4.1143	0.8625	18.09	49.41
17	M3	0.056	1.3	35.6112	27.4674	–30.80	1573.78

Table 4. Results of harmonic analysis of observation in 1999–2000. Extensometer EW–2.

	Wave group	Amplitude measured, nstr	Ratio signal/noise	Amplitude factor and its r.m.s.e.		Phase lead, deg. and its r.m.s.e.	
1	Q1	0.841	16.0	0.6640	0.0415	–6.09	2.33
2	O1	4.920	92.1	0.7436	0.0081	1.95	0.46
3	M1	0.741	10.5	1.4230	0.1358	–36.96	7.04
4	P1	2.507	51.0	0.8142	0.0160	64.32	0.91
5	S1	2.397	34.7	32.9259	0.9500	–73.56	54.46
6	K1	5.176	97.3	0.5562	0.0057	28.23	0.33
7	PSI1	0.602	12.1	8.2650	0.6809	13.33	39.02
8	PHI1	0.812	16.2	6.1258	0.3782	–44.23	21.67
9	J1	0.522	10.4	1.0026	0.0965	–9.00	5.57
10	OO1	0.457	6.7	1.6037	0.2384	–34.28	13.66
11	2N2	0.068	1.5	4.3796	2.9713	–154.20	170.26
12	N2	0.238	3.9	2.4352	0.6166	97.94	35.32
13	M2	0.495	10.5	0.9685	0.0926	5.83	5.49
14	L2	0.081	2.7	3.2416	1.1929	95.56	68.35
15	S2	1.707	34.8	7.1766	0.2064	–99.45	11.41
16	K2	0.260	4.7	4.0196	0.8602	20.14	49.28
17	M3	0.082	1.9	51.8937	27.36890	–25.94	1568.17

Table 5. Results of harmonic analysis of observation in 1999–2000. Extensometer EW–3.

	Wave group	Amplitude measured, nstr	Ratio signal/noise	Amplitude factor and its r.m.s.e.		Phase lead, deg. and its r.m.s.e.	
1	Q1	0.769	14.9	0.6067	0.0407	–6.37	2.08
2	O1	5.108	96.5	0.7720	0.0080	1.55	0.46
3	M1	0.727	10.2	1.3970	0.1368	–30.59	7.93
4	P1	2.582	52.7	0.8386	0.0159	63.29	0.91
5	S1	2.303	33.3	31.6374	0.9514	–78.68	54.53
6	K1	5.242	99.0	0.5633	0.0057	25.07	0.33
7	PSI1	0.560	11.3	7.6904	0.6819	-4.44	39.07
8	PHI1	0.721	14.4	5.4414	0.3767	–48.06	21.58
9	J1	0.473	9.6	0.9086	0.0948	–0.45	5.26
10	OO1	0.440	6.4	1.5467	0.2417	–30.90	13.85
11	2N2	0.115	2.5	7.3522	2.9357	-129.32	168.21
12	N2	0.207	3.5	2.1146	0.6097	104.08	34.93
13	M2	0.368	7.8	0.7202	0.0921	–33.30	5.51
14	L2	0.076	2.6	3.0328	1.1753	110.88	67.35
15	S2	1.840	37.9	7.7354	0.2043	-98.77	11.70
16	K2	0.251	4.6	3.8798	0.8495	21.98	48.67
17	M3	0.088	2.1	56.0900	27.2240	–25.62	1559.83

Table 6. Tidal parameters from three parallel extensometer at Protvino.

Wave group	Amplitude, nstr			Phase lead, degree		
	EW–1	EW–2	EW–3	EW–1	EW–2	EW–3
Q1	0.832	0.841	0.769	–5.69	–6.09	–6.37
O1	4.874	4.920	5.108	2.86	1.95	1.55
M1	0.809	0.741	0.727	–27.85	–36.96	–30.59
P1	2.514	2.507	2.582	65.62	64.32	63.29
S1	2.202	2.397	2.303	–75.40	–73.56	–78.68
K1	5.192	5.176	5.242	28.89	28.23	25.07
PSI1	0.549	0.602	0.560	0.83	13.33	-4.44
PHI1	0.834	0.812	0.721	–39.34	–44.23	–48.06
J1	0.538	0.522	0.473	–9.49	–9.00	–0.45
OO1	0.394	0.457	0.440	–33.22	–34.28	–30.90
2N2	0.064	0.068	0.115	–132.62	–154.20	-129.32
N2	0.256	0.238	0.207	108.17	97.94	104.08
M2	0.547	0.495	0.368	5.26	5.83	–33.30
L2	0.110	0.081	0.076	93.79	95.56	110.88
S2	1.630	1.707	1.840	–99.80	–99.45	-98.77
K2	0.266	0.260	0.251	18.09	20.14	21.98
M3	0.056	0.082	0.088	–30.80	–25.94	–25.62

Table 7. Results of harmonic analysis of observation in 1999–2000 with compensation of temperature and atmospheric pressure variations.

Component, extensometer	Amplitude, nstr		Ratio of amplitude factors		Standard residual, nstr	Response	
	O1	S1	$\varphi_{P1} / \varphi_{O1}$	$\varphi_{K1} / \varphi_{O1}$		Temperat.	Pressure
No weather effects accounted							
NS–1	2.920	3.088	1.014 ±0.035	0.371 ±0.012	3.444	—	—
EW–1	4.874	2.202	1.108 ±0.025	0.757 ±0.011	3.958	—	—
EW–2	*4.920*	*2.397*	*1.095 ±0.024*	*0.748 ±0.011*	*3.944*	—	—
EW3	**5.108**	**2.303**	**1.086 ±0.024**	**0709 ±0.010**	**3.973**	—	—
With response to outer temperature							
NS–1	2.913	0.990	0.404 ±0.030	0.528 ±0.135	3.176	–0.941	—
EW–1	4.875	0.695	1.101 ±0.024	0.823 ±0.012	3.833	–0.688	—
EW–2	*4.926*	*0.554*	*1.103 ±0.024*	*0.813 ±0.012*	*3.757*	*–0.706*	—
EW–3	**5.103**	**0.943**	**1.106 ±0.023**	**0.803 ±0.011**	**3.813**	**–0.782**	—
With response to atmospheric pressure							
NS–1	3.004	2.932	0.930 ±0.030	0.345 ±0.012	3.390	—	0.890
EW–1	4.935	2.054	1.044 ±0.024	0.740 ±0.011	3.929	—	0.699
EW–2	*4.985*	*2.249*	*1.029 ±0.024*	*0.729 ±0.011*	*3.912*	—	*0.737*
EW–3	**5.190**	**2.130**	**1.012 ±0.023**	**0.709 ±0.010**	**3.928**	—	**0.872**
With response to outer temperature and atmospheric pressure							
NS–1	2.958	0.817	0.367 ±0.030	0.502 ±0.013	3.159	–0.890	0.485
EW–1	4.899	0.582	1.067 ±0.024	0.810 ±0.011	3.832	-0.644	0.386
EW–2	*5.121*	*0.461*	*1.065 ±0.024*	*0.799 ±0.012*	*3.938*	*-0.680*	*0.442*
EW–3	**5.175**	**0.774**	**1.054 ±0.022**	**0.780 ±0.011**	**3.800**	**–0.720**	**0.530**
NS	Rated value		0.90	0.65			
EW			0.94	0.80			

Table 8. Elimination of outer temperature effect from measured deformation waves P_1 and K_1 for component NS, 1999–2000
(assuming that temperature affects these waves the same way as S_1)

		P1		S1		K1	
		A	κ	A	κ	A	κ
1	Theoretical value	1.939	0.0	0.046	0.0	5.862	0.0
2	Measured deformation, nstr (tide + temperature effect)	1.378	124.6	3.088	–65.6	1.522	39.6
3	Measured temperature, C°	1.088	–35.1	4.104	107.2	1.190	–31.7
4	The same A_T and κ_T after the subtracting 180° from phases	–1.088	144.9	–4.104	–72.8	–1.190	148.3
5	Response for S1: [row 2] / [row 4] and shift of phase: [2] minus [4]			–0.7524	7.2		
6	Estimated deformation induced by temperature: $A = -0.7524\,A_T$; $\kappa = \kappa_T + 7.2$	0.819	152.2	3.088	–65.6	0.895	155.6
7	Deformation without temperature effect: [2] minus [6]	0.755	94.5	0.000	—	2.077	16.8
8	Amplitude factor: [7] / [0]	0.389				0.354	
9	Amplitude factor divided by that for wave O1: [8] / 0.701	0.556				0.506	
10	Rated value for ε_{P1} and ε_{K1}	0.90				0.65	

Table 9. Comparison of the different methods of temperature correction (NS component)

Method (criteria)		τ (hour)	R (nstr/K)	s_0 (nstr)	A_{S1} (nstr)	ε_{P1}	ε_{K1}	K_{K1} (°)
Without account of temperature		—	—	3.444	3.088	0.404	0.528	39.6
With Account of the integral temperature effect		–2.0	–0.721	3.288	1.200	0.785	0.546	24.9
	Maximum ε_{K1}	–1.0	–0.856	3.223	0.615	0.604	0.550	17.5
	Minimum A_{S1}	–0.8	–0.879	3.210	0.601	0.565	0.547	16.0
		0.0	–0.941	3.176	0.890	0.404	0.528	10.2
	Maximum R, minimum s_0	0.6	–0.956	3.168	1.472	0.327	0.501	6.7
		1.0	–0.951	3.171	1.569	0.266	0.478	4.3
	Minimum κ_{K1}	2.0	–0.873	3.215	2.183	0.345	0.407	1.9
		3.0	–0.714		3.293	0.548	0.336	5.9
Temperature and its derivative		0.56	-0.973	3.162	1.318	0.299	0.506	6.2
Elimination of S1 (see Table 8)		–0.48	–0.752	—	0.000	0.566	0.506	16.8

Note: The values for $\tau = -0.8$ and $\tau = 0.6$ are taken from approximations by parabolas based on nearest 4–5 values derived from Eterna program (Fig. 5).

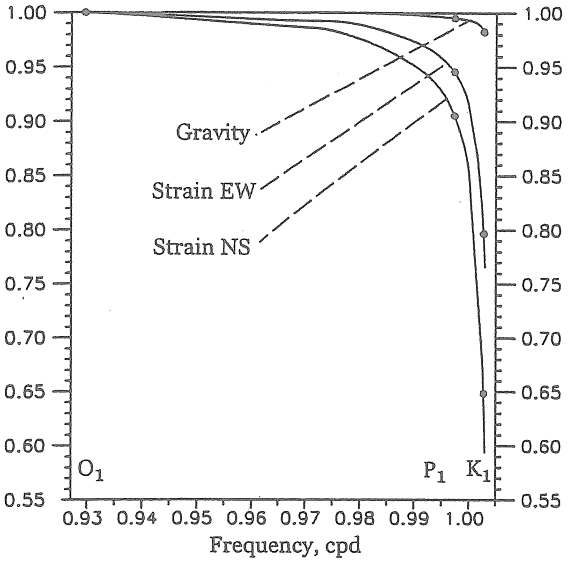

Fig. 1. Relative diminution of tide wave amplitude owing to the liquid core resonanse, according to Wahr [1981].

Fig. 2

Sketch of the Protvino underground station

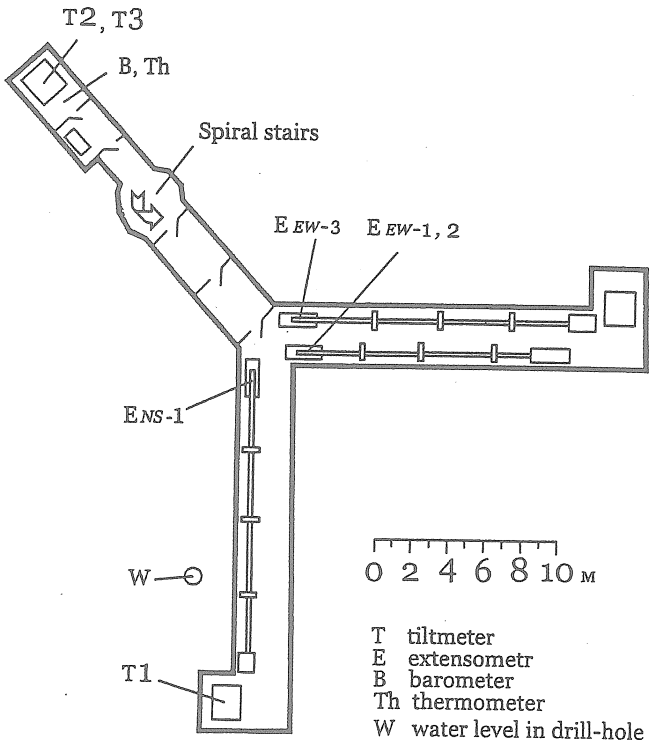

Fig. 3. Spectrum of inside temperature, C°

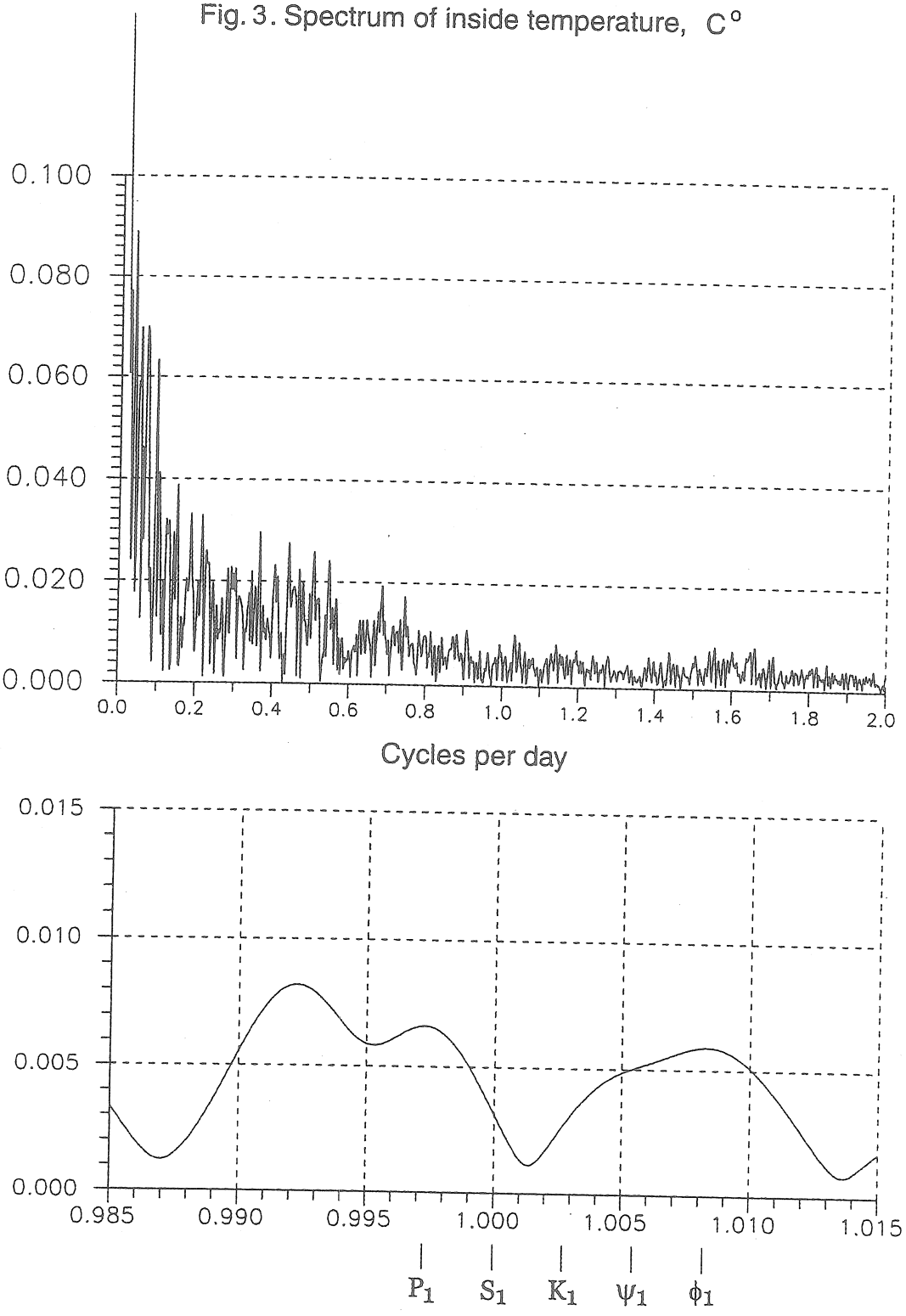

Fig. 4. Spectrum of temperature at weather station Serpukhov for three years 1998-2000

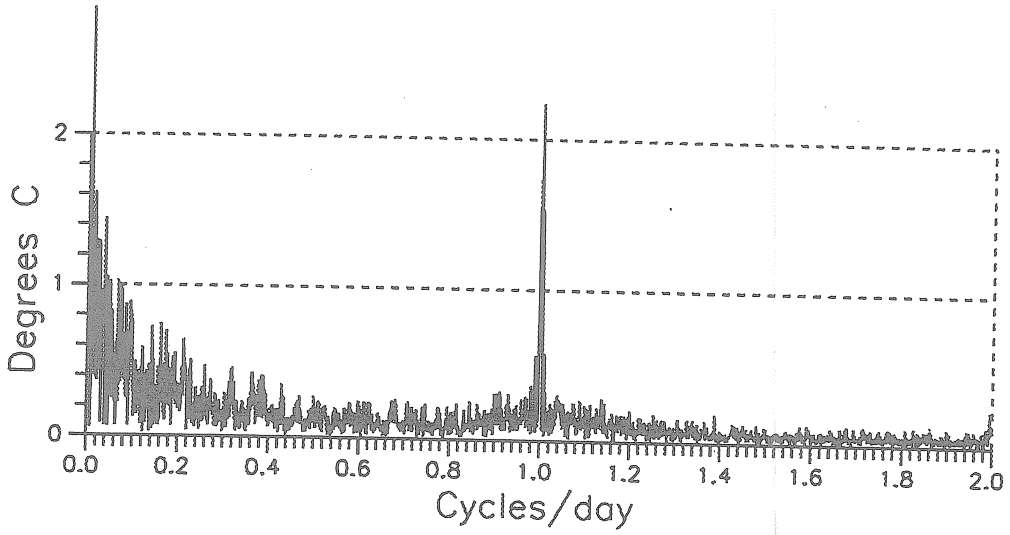

Dash line: SPECRTUM OF MODEL WAVE S1
Amplitude=3.0 modulated by the wave
with period 365.25 days and amplitude 1.5

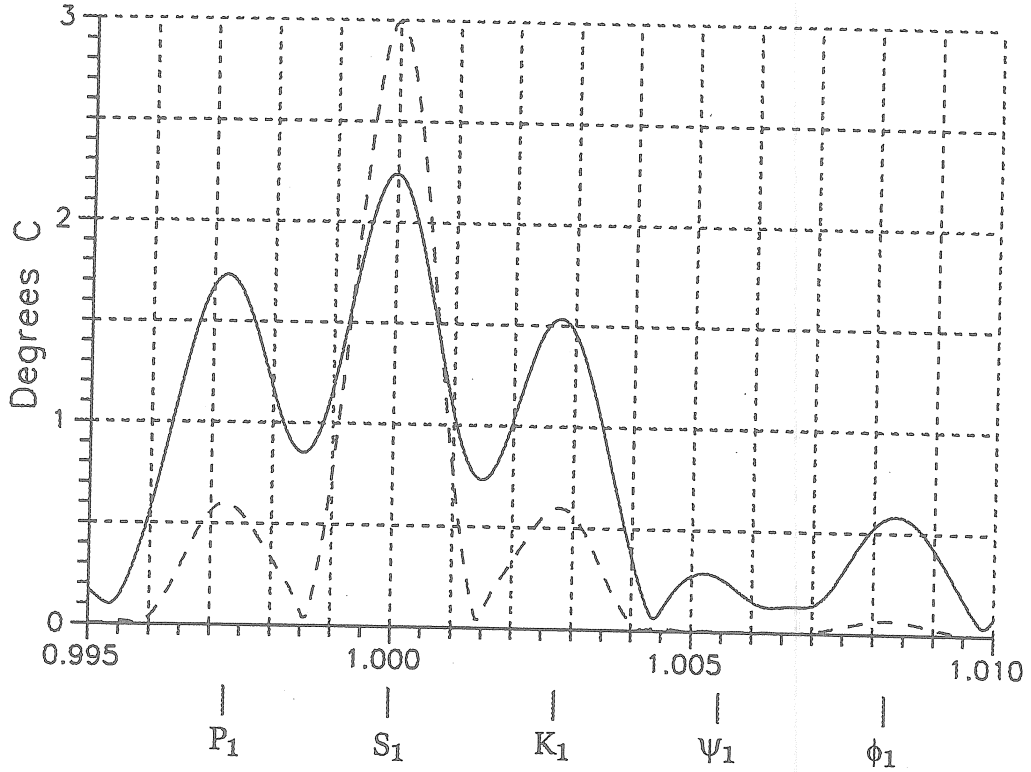

Fig. 5

Temperature compensation of NS–1 deformations at various time shift of temperature

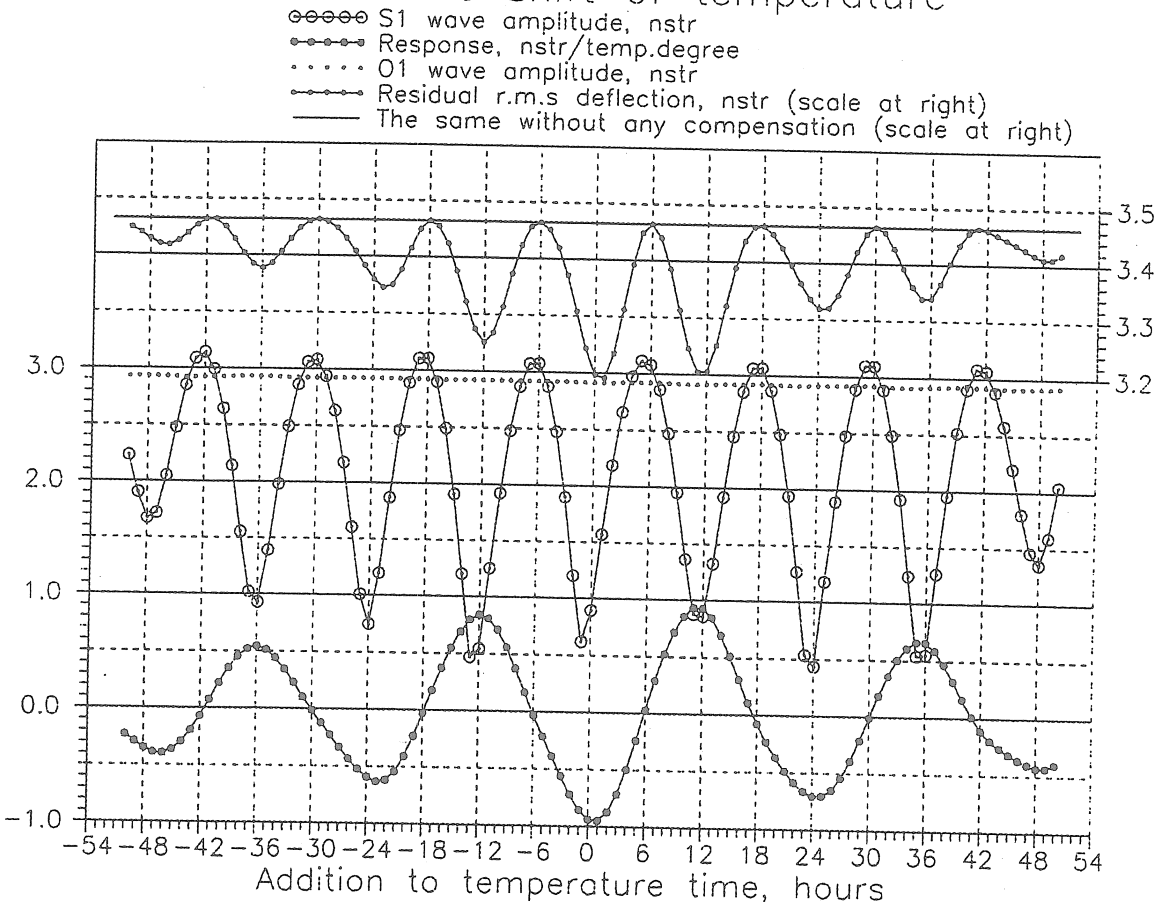

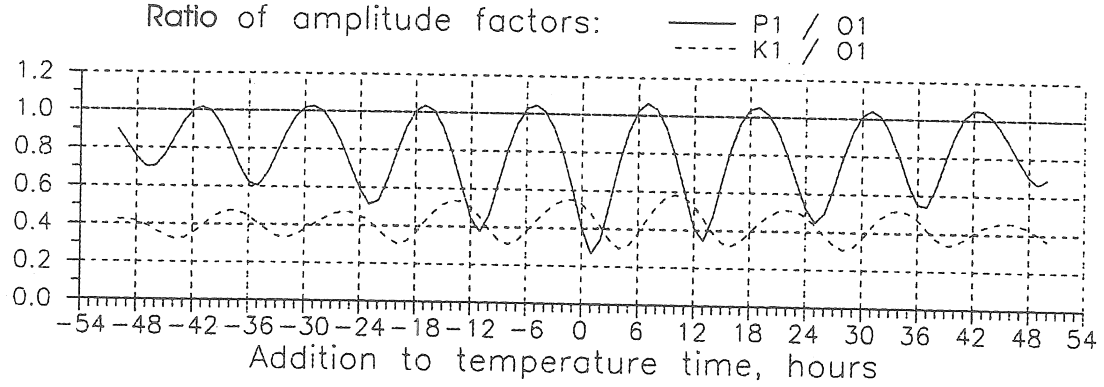

Fig.6.

Temperature compensation of EW–3 deformations at various time shift of temperature

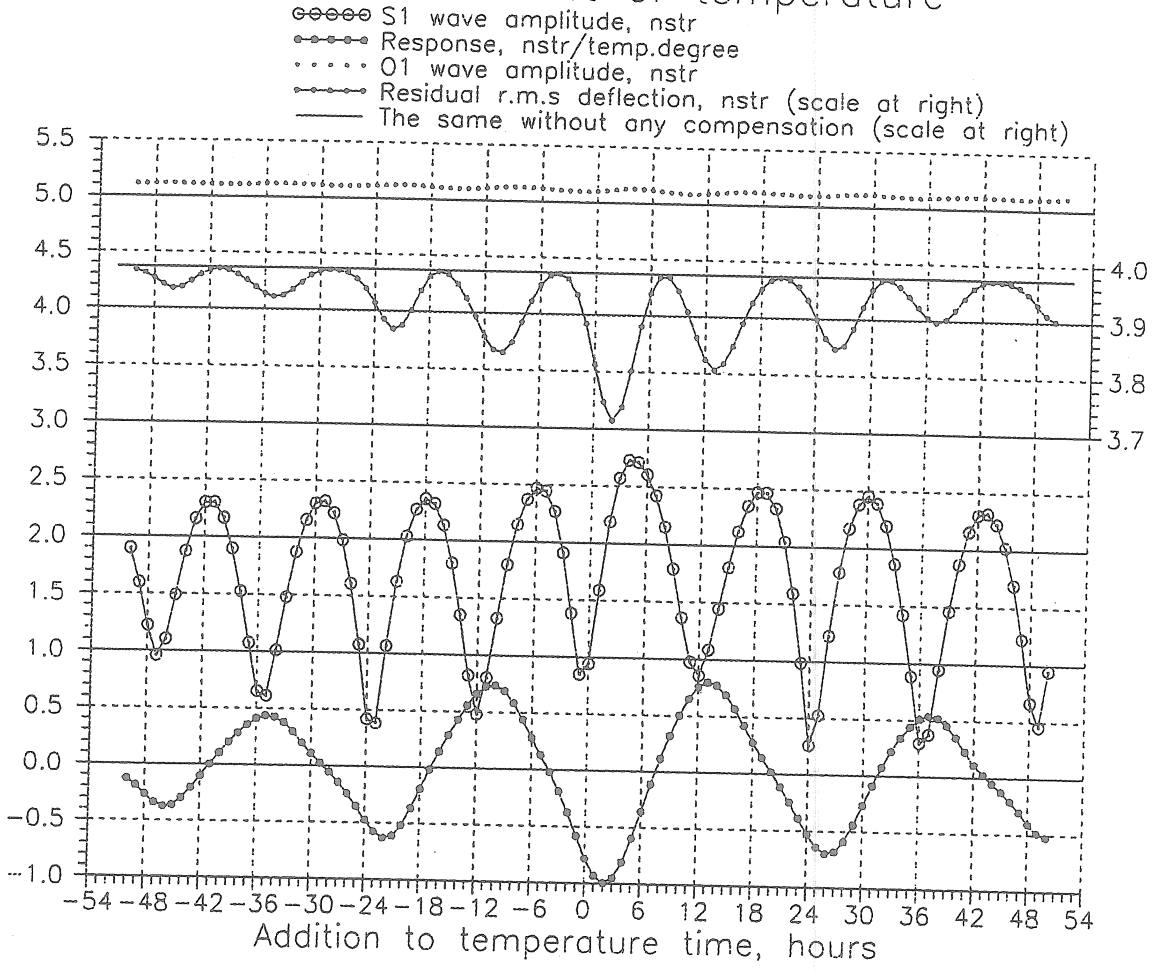

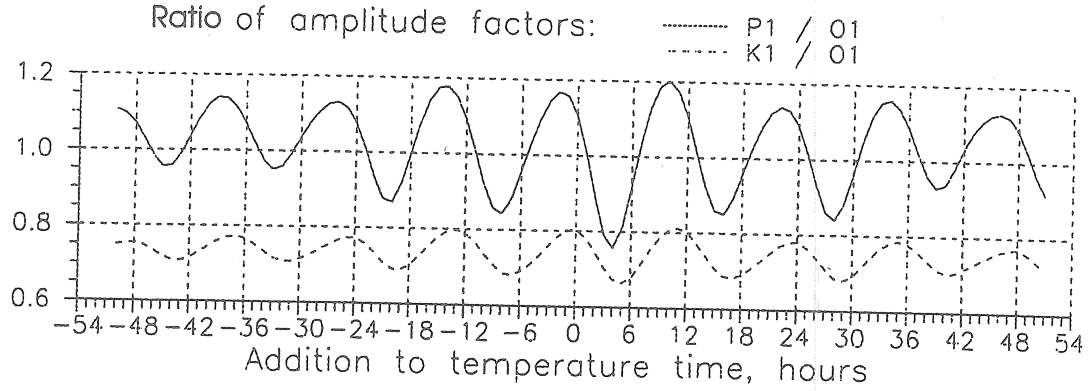

Fig. 7

Vectorial diagram illustrating the correction method based on the elimination of S_1

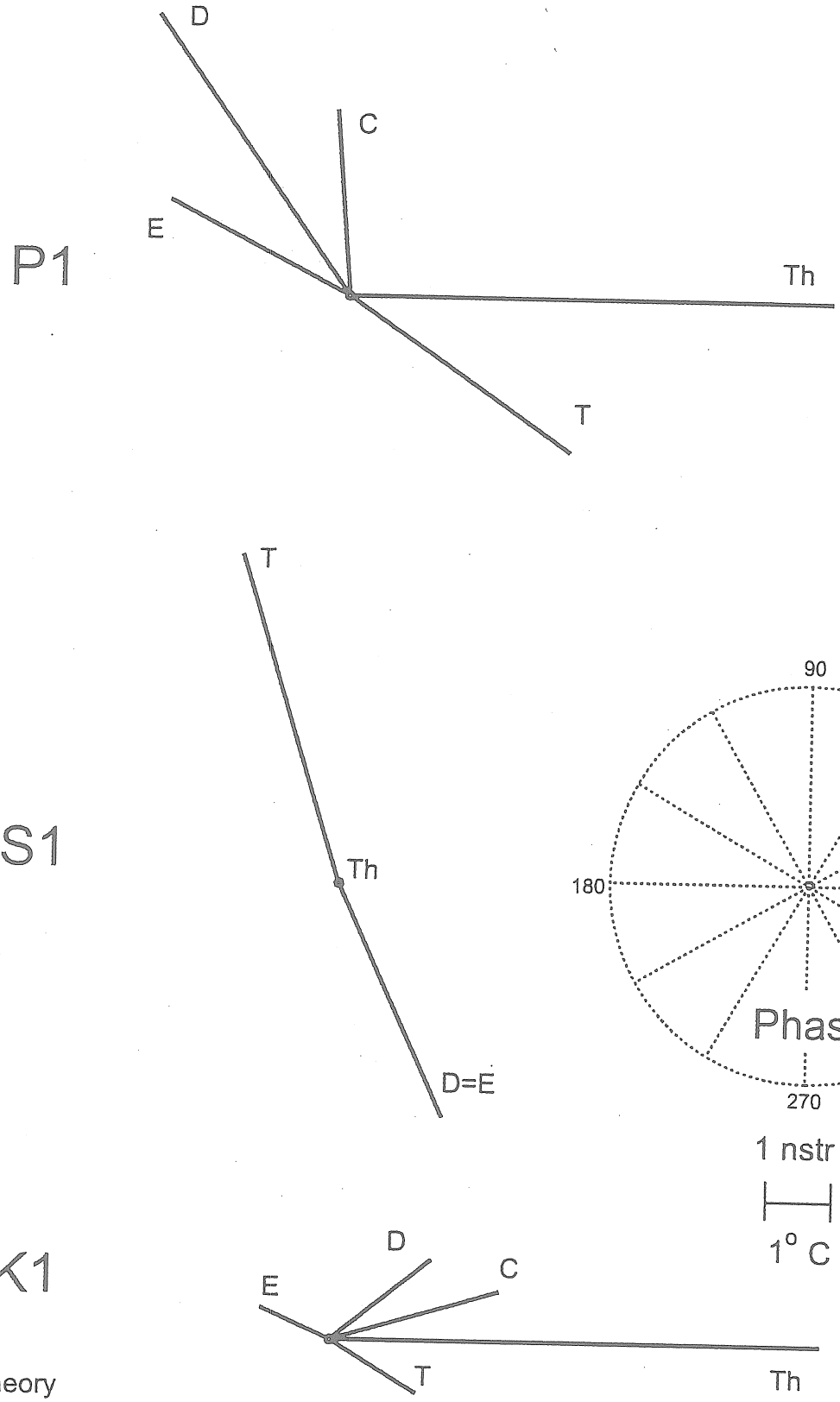

Th - Theory
D - Deformation measured
T - Temperature
E - Effect of temperature on deformation
C - "Cleaned" deformation